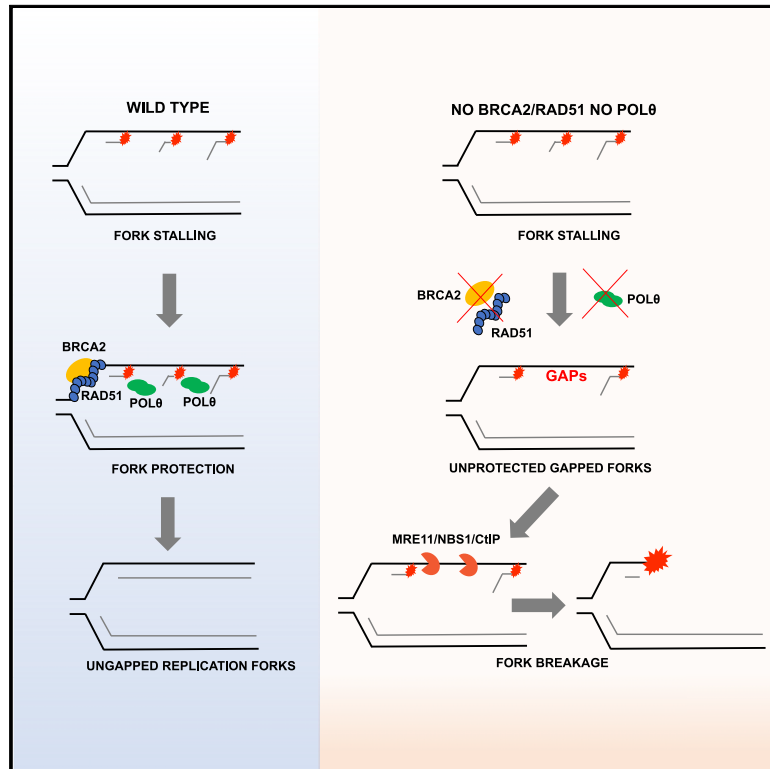# POLθ prevents MRE11-NBS1-CtIP-dependent fork breakage in the absence of BRCA2/RAD51 by filling lagging-strand gaps

Graphical abstract

Authors

Anjali Mann,
Miguel Angel Ramirez-Otero,
Anna De Antoni, ..., Sara Bernardo,
Joanna Loizou, Vincenzo Costanzo

Correspondence

vincenzo.costanzo@ifom.eu

In brief

In this study, Mann et al. discover that POLθ protects the vertebrate genome from the accumulation of DNA gaps, which can lead to chromosome breakage in the absence of BRCA2/RAD51. This novel function of POLθ promotes BRCA2-defective cancer cell survival and can be targeted with a specific inhibitor.

Highlights

- POLθ is recruited onto stalled replication forks preventing ssDNA gaps and breakage

- POLθ polymerase extends stalled OKFs, whereas POLθ helicase removes them

- POLθ complements the absence of BRCA2/RAD51 at replication forks

- POLθ prevents MRE11-NBS1-CtIP endonuclease-dependent fork breakage

CellPress

Article

POLθ prevents MRE11-NBS1-CtIP-dependent fork breakage in the absence of BRCA2/RAD51 by filling lagging-strand gaps

Anjali Mann,[1,2] Miguel Angel Ramirez-Otero,[1,2] Anna De Antoni,[1] Yodhara Wijesekara Hanthi,[1,2] Vincenzo Sannino,[1,2] Giorgio Baldi,[1,2] Lucia Falbo,[1,2] Anna Schrempf,[3] Sara Bernardo,[3] Joanna Loizou,[3] and Vincenzo Costanzo[1,2,4,*]

[1]IFOM ETS, The AIRC Institute of Molecular Oncology, Milan, Italy
[2]Department of Oncology and Hematology-Oncology, University of Milan, Milan, Italy
[3]Institute of Cancer Research, Department of Medicine I, Comprehensive Cancer Centre, Medical University of Vienna, Vienna, Austria
[4]Lead contact
*Correspondence: vincenzo.costanzo@ifom.eu
https://doi.org/10.1016/j.molcel.2022.09.013

SUMMARY

POLθ promotes repair of DNA double-strand breaks (DSBs) resulting from collapsed forks in homologous recombination (HR) defective tumors. Inactivation of POLθ results in synthetic lethality with the loss of HR genes BRCA1/2, which induces under-replicated DNA accumulation. However, it is unclear whether POLθ-dependent DNA replication prevents HR-deficiency-associated lethality. Here, we isolated *Xenopus laevis* POLθ and showed that it processes stalled Okazaki fragments, directly visualized by electron microscopy, thereby suppressing ssDNA gaps accumulating on lagging strands in the absence of RAD51 and preventing fork reversal. Inhibition of POLθ DNA polymerase activity leaves fork gaps unprotected, enabling their cleavage by the MRE11-NBS1-CtIP endonuclease, which produces broken forks with asymmetric single-ended DSBs, hampering BRCA2-defective cell survival. These results reveal a POLθ-dependent genome protection function preventing stalled forks rupture and highlight possible resistance mechanisms to POLθ inhibitors.

INTRODUCTION

Maintenance of replication fork integrity is essential for cell survival and genome stability. Numerous DNA repair factors participate in DNA replication under normal and stressful conditions. Among these, homologous recombination (HR) proteins RAD51, BRCA1, and BRCA2 play a major role in preventing the accumulation of single-stranded (ss) DNA gaps during DNA replication (Cantor, 2021; Chen et al., 2018; Cong et al., 2021; Feng and Jasin, 2017; Hashimoto et al., 2010; Kolinjivadi et al., 2017a, 2017b; Taglialatela et al., 2017, 2021). Mechanisms underlying ssDNA accumulation in the absence of HR proteins in part rely on the degradation of nascent DNA at stalled forks initiated by MRE11 (Hashimoto et al., 2010). Such processing can lead to the formation of small ssDNA gaps behind replication forks and extensive nascent DNA degradation triggered by SMARCAL1 and other SNF2-like translocases in the context of fork reversal (Quinet et al., 2017b). Nuclease-independent ssDNA gaps at replication fork junctions have also been described in the absence of HR proteins bound to chromatin (Hashimoto et al., 2010; Kolinjivadi et al., 2017b).

The function of HR proteins in DNA replication has been shown to be essential for cell survival and has been linked to PARP inhibitor sensitivity (Cantor, 2021; Cong and Cantor, 2022; Pan-

zarino et al., 2021). These roles are distinct from the classical HR-mediated metabolism of DSBs, which can also be repaired through covalent joining of DNA ends by other highly efficient pathways, including classical nonhomologous end-joining (C-NHEJ) and alternative-NHEJ (alt-NHEJ) (Chang et al., 2017; Schrempf et al., 2021). Genome sequence analysis of HR-defective tumors has revealed DNA rearrangements in part due to polymerase θ (POLθ)-dependent alt-NHEJ (Schrempf et al., 2021). Consistent with this, inactivation of POLθ-encoding gene *POLQ* is synthetically lethal with defects in genes controlling HR (Brambati et al., 2020; Ceccaldi et al., 2015; Mateos-Gomez et al., 2015).

POLθ is a large protein containing a low fidelity A-family polymerase (POL) domain at the C terminus and a helicase domain at the N terminus joined by a nonstructured central region. The role of POLθ in alt-NHEJ is well established (Wood and Doublié, 2016). POLθ has also been shown to promote symmetric fork progression, suggesting an additional function during DNA replication (Ceccaldi et al., 2015). However, apart from DSB repair, POLθ's function remains poorly characterized. In particular, it is not known whether the ability of POLθ to support HR-defective cell survival is linked to its replicative role, which might not leave any detectable genomic scar.
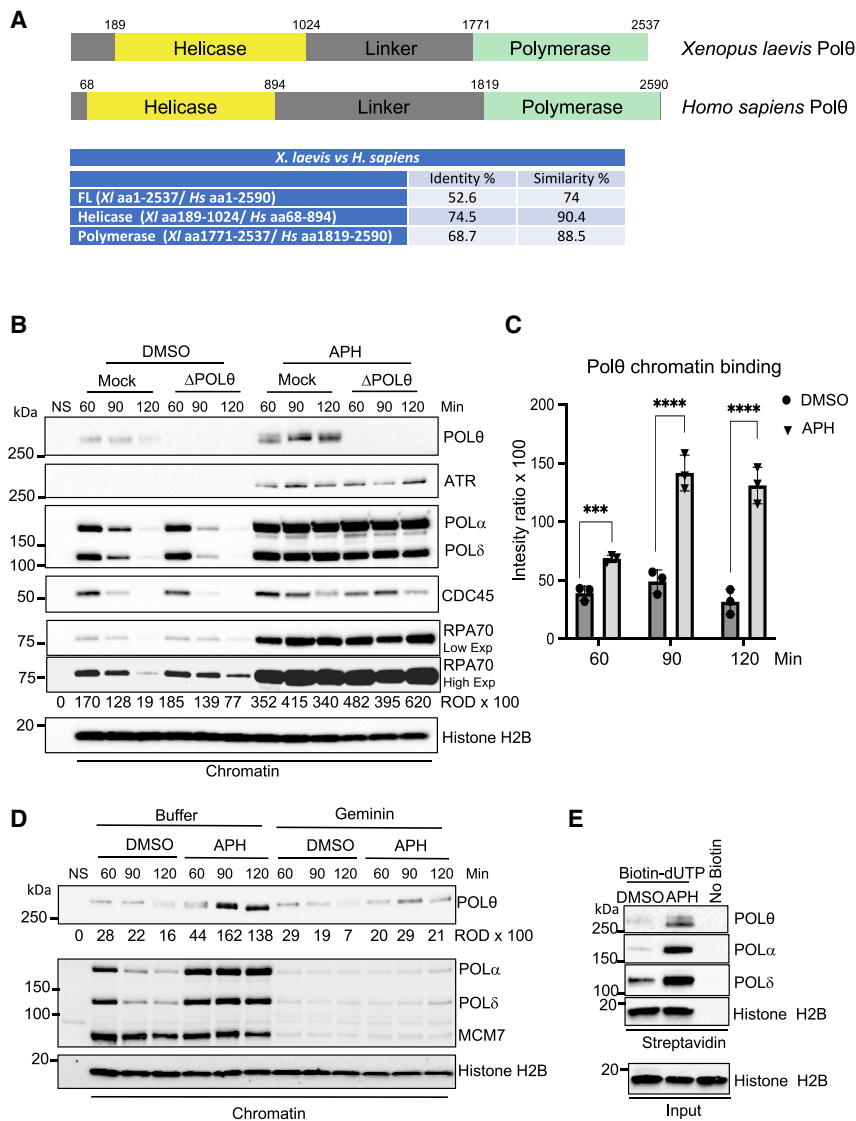
A

X. laevis vs H. sapiens	Identity %	Similarity %
FL (*Xl* aa1-2537/ *Hs* aa1-2590)	52.6	74
Helicase (*Xl* aa189-1024/ *Hs* aa68-894)	74.5	90.4
Polymerase (*Xl* aa1771-2537/ *Hs* aa1819-2590)	68.7	88.5

B

C

Polθ chromatin binding

D

E

Figure 1. *Xenopus* POLθ is recruited to stalled replication forks

(A) *Human* and *Xenopus* POLθ.

(B) Representative western blot (WB) of chromatin-binding time course of mock and POLθ-depleted extracts treated with DMSO or APH (1.5 mM). Chromatin isolation time points following nuclei addition to egg extracts are indicated. Chromatin-bound RPA quantification was determined by relative optical density (ROD) compared with histone H2B.

(C) POLθ chromatin-binding ratio with histone H2B. Columns indicate mean ± SD; n = 3; unpaired t test; ***p < 0.001; ****p < 0.0001.

(D) Representative WB of the indicated proteins from DMSO or APH-treated extracts supplemented with buffer or geminin. ROD for the POLθ band compared with H2B is indicated.

(E) Representative iPOND experiment showing nascent chromatin isolated from extracts treated with DMSO or APH 60 min after nuclei addition in the presence or absence of biotin-dUTP added 10 min earlier.

See also Figure S1.

The investigation of BRCA-defective tumor sensitivity caused by replicative defects is emerging as a key area to identify possible targets that induce synthetic lethality when inactivated (Cantor, 2021; Cong et al., 2021; Quinet et al., 2020; Taglialatela et al., 2021; Tirman et al., 2021). However, the molecular mechanisms underlying synthetic lethality remain poorly understood. This is in part due to the lethality of BRCA1 and BRCA2 deletion in normal cells, which limits in-depth molecular analysis. This obstacle can be overcome by cell-free extracts from *Xenopus laevis* eggs that allow for the manipulation of large protein complexes in their physiological context, thus recapitulating DNA repair proteins function during chromosomal DNA replication (Aze et al., 2016). Over the years, the use of this system has highlighted unexpected functions of HR proteins in DNA replication that have been extensively validated in mammalian cells (Costanzo and Gautier, 2004; Hashimoto and Costanzo, 2011; Raspelli et al., 2017; Sannino et al., 2016, 2017).

To investigate the role of POLθ in an HR-defective context overcoming cell lethality, we have isolated the *Xenopus laevis* POLθ ortholog and studied its function in chromosomal DNA replication. Here, we report that POLθ plays a major role in replication fork metabolism under stressful conditions. Using DNA electron microscopy (EM), we show that POLθ suppresses the accumulation of ssDNA fork gaps arising at stalled forks. This is achieved by POLθ-mediated filling of ssDNA through its POL domain, which extends stalled Okazaki fragments (OKFs), directly visualized here. Consistent with these findings, POLθ polymerase inhibition leads to the accumulation of ssDNA gaps that predispose to the formation of MRE11-dependent DSBs in HR-defective cells mainly during the S-phase. These results provide unexpected molecular and DNA structural mechanisms underlying POLθ's function in DNA replication in the absence of functional HR proteins.

RESULTS

Isolation and characterization of *Xenopus laevis* POLθ

Using maternal *Xenopus laevis* cDNA, we isolated *Xenopus laevis* POLθ (Figure S1A), which has highly conserved helicase and polymerase domains (Figures 1A and S1B). POLθ full length (POLθ-FL), polymerase (POLθ-POL), and helicase containing (POLθ-HEL) polypeptides were cloned, expressed, and purified (Figure S1C). A large POLθ C terminus domain served as antigen to produce rabbit polyclonal antibodies that recognized a band of the predicted size in egg extracts (Figure S1D).

Using anti-*Xenopus* POLθ antibodies, we showed that POLθ binds to chromatin during DNA replication (Figure 1B). Recombinant POLθ-FL was also able to bind replicating chromatin (Figure S1E). Remarkably, chromatin recruitment of POLθ was strongly increased by stalled forks induced by replicative DNA polymerase inhibitor aphidicolin (APH) (Wist and Prydz, 1979) (Figures 1B–1D) similar to other APH-responding proteins such as ATR, polymerase alpha (POLα), polymerase delta (POLδ), and replication protein A (RPA) (Figures 1B and 1C). POLθ depletion (Figure 1B) did not impair the loading of general replication factors or stalled forks responding proteins. However, the absence of POLθ led to increased and persistent chromatin binding of RPA even in the absence of APH, suggesting the accumulation of ssDNA (Figure 1B). Importantly, POLθ increased chromatin binding was inhibited by geminin, an inhibitor of replication origin assembly (McGarry and Kirschner, 1998), which prevents chromatin loading of replisome components (Figure 1D). The binding of POLθ to APH-induced stalled forks was confirmed by the isolation of nascent proteins bound to DNA (iPOND) (Dungrawala and Cortez, 2015; Sirbu et al., 2013) (Figure 1E).

Defective replication intermediates recruiting POLθ
Studying the effects of APH on POLθ DNA POL activity, we found that although POLθ-FL and POLθ-POL were able to elongate a synthetic DNA primer containing a 3′-OH end annealed to a ssDNA template (Figure S2A), increasing APH amounts did not inhibit their DNA polymerase activity (Figure S2B), similar to other APH-insensitive A-family polymerases (Seki et al., 2003). Therefore, increased binding of POLθ to stalled forks was not due to the inhibition of its DNA polymerase activity in contrast to APH-inhibited B-family POLδ and POLα (Wist and Prydz, 1979) (Figures 1B–1D). Consistent with the ability of POLθ helicase domain to displace oligos annealed to ssDNA *in vitro* (Ozdemir et al., 2018), POLθ-FL was able to synthesize DNA past an annealed oligo, although with low efficiency. In contrast, T4 POL, which lacks helicase activity (Challberg and Englund, 1980), was completely blocked by the annealed oligo (Figure S2C).

To identify the DNA structures inducing POLθ chromatin recruitment, we analyzed replication intermediates (RIs) isolated from interphase extracts using DNA EM (Hashimoto and Costanzo, 2011; Sannino et al., 2017), which provides snapshot images of psoralen-cross-linked DNA molecules (Kolinjivadi et al., 2017b; Taglialatela et al., 2017, 2021). For the analysis, we considered replication bubbles and Y-shaped RIs obtained by restriction digestion, which produces two replicated branches of similar lengths allowing to distinguish them from the parental strand (Sannino et al., 2017).

RIs isolated from untreated extracts showed minimal amounts of ssDNA, usually below 150 nucleotides (nt) in length, present at fork junctions and mostly localized on one of the daughter strands (Figure 2A), when visible, as previously reported (Kolinjivadi et al., 2017b).

Instead, high doses of APH added to extracts during DNA replication 60 min after sperm nuclei supplementation, followed by 45-min incubation, induced the formation of RIs bearing long tracts of ssDNA at replication fork junctions. ssDNA was present only on one of the daughter strands (Figure 2B), conferring an asymmetric configuration to stalled forks.

To confirm that the structures observed were present endogenously and were not artifacts of the EM procedure, we performed denaturing EM in which psoralen-cross-linked DNA is heat denatured before spreading. This procedure reveals DNA packaged with nucleosomes (nucleosomal DNA) resistant to psoralen-cross-linking and therefore more prone to denaturation (Cech et al., 1978). Limited amount of ssDNA was present on daughter strands at fork junctions adjacent to nucleosomal DNA in unchallenged conditions (Figure S3A). APH, instead, induced long asymmetric ssDNA segments adjacent to the denatured nucleosomal DNA (Figure S3B). These results indicate that RIs observed in nondenaturing conditions reflect endogenous replicating chromatin structures.

In addition to RIs with ssDNA, we detected reversed forks (Kolinjivadi et al., 2017b) (Figure S3C), which were also made of nucleosomal DNA (Figure S3D).

To better understand the mechanisms leading to the formation of asymmetric ssDNA gaps, we tested the possible role of nucleases MRE11 and DNA2 in generating them. We observed that most of the ssDNA gaps were insensitive to nuclease inhibition although rare large gaps above 2,000 nt in length could be reduced by MRE11 or DNA2 exonuclease inhibitors (Mirin and DNA2i, respectively) (Figure S4A). These results indicate that the observed gaps were largely independent of these nucleases when using sperm nuclei as templates.

As APH also induces reversed forks containing DNA ends to which POLθ could bind, we tested the impact of inhibiting reversed fork formation on POLθ chromatin loading. We depleted SMARCAL1, the removal of which strongly inhibits reversed fork formation in egg extracts. However, SMARCAL1 depletion (Kolinjivadi et al., 2017b) did not affect POLθ chromatin binding (Figure S4B) although it inhibited the formation of more than ~70% of APH-induced reversed forks (Figure S4C). These results indicate that structures containing DNA ends such as reversed forks are not responsible for enhanced POLθ recruitment to chromatin promoted by APH-induced fork stalling.

Accumulation of ssDNA gaps is induced by stalled OKFs
To better understand the process leading to ssDNA formation and the potential effect of POLθ on this substrate, we developed a method to distinguish continuous leading-strand polymerization from discontinuous lagging-strand DNA synthesis at fork junctions. Moderate amounts of APH (20 μM, M-APH) added to egg extract 60 min after sperm nuclei and incubated for 45 min yielded RIs with one discontinuous daughter strand in which ssDNA gaps alternated with double-stranded DNA (dsDNA) fragments (Figures 2C–2F and S4D–S4G). In contrast to uninterrupted fork junction gaps induced by high doses of APH, the length of which was ~1,200 nt, reaching 3,000–4,000 in some cases (Figures 2B and 2F), we could detect from 1 up to 4 ssDNA gaps measuring ~400 nt on average (Figures 2C–2F). These gaps were separated by dsDNA ranging from 100 to 350 nt in size, which likely correspond to stalled OKFs synthesized by POLα and POLδ (Pellegrini, 2012) (Figure 2G). These results are compatible with discontinuous DNA synthesis taking place on the lagging strand. Similar to higher doses of APH, M-APH levels did not induce the accumulation of ssDNA gaps on the opposite strand (Figures 2C–2F and S4D–S4G). Given
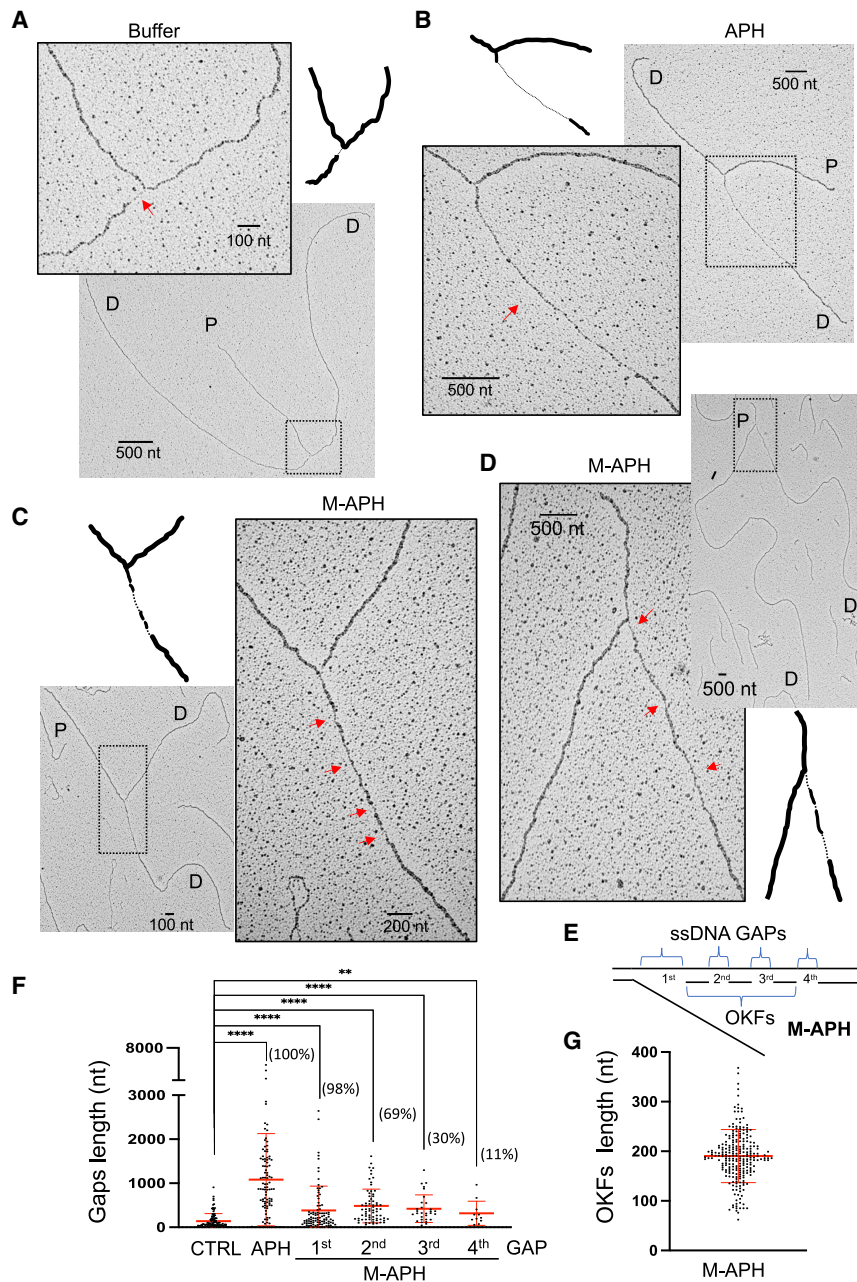
Figure 2. Replicative polymerases inhibition induces stalled OKFs detected by EM

(A and B) (A) Representative EM images of RIs isolated from an extract treated with DMSO-containing buffer or (B) 1.5 mM aphidicolin (APH) added 60 min after nuclei addition to extracts and incubated for additional 45 min. Letters indicate daughter (D) and parental (P) strands. Outlined windows show the magnified section highlighted in dotted rectangle. Schematic drawings represent dsDNA (continuous line) and ssDNA (dotted line) thickness, respectively. Bar lengths in nucleotides (nt) are indicated. Red arrows highlight ssDNA.

(C and D) Representative replication forks isolated following 20 μM APH (M-APH) added to the extract as in (B) showing OKFs separated by ssDNA.

(E) Scheme showing asymmetric ssDNA gap distribution.

(F) Gap quantification of DNA molecules represented in (A), (B), (C), and (D). Each dot represents the gap length for each RI isolated from extracts treated as indicated. Horizontal axis numbers indicate gap position from fork junction as in (E) for the same RI containing 1, 2, 3, or 4 gaps. Measurements were conducted on 300 RIs pooled from three independent experiments (n = 300); 100 RIs were counted for each treatment; horizontal bars indicate mean ± SD; unpaired t test; **p < 0.01;****p < 0.0001. Percentage of RIs with APH- and M-APH-induced-gaps is indicated in parentheses.

(G) OKF length detected on RIs isolated from extracts treated with M-APH as in (C) and (D). Measurements were conducted on RIs pooled from independent experiments (n = 100). Horizontal bars indicate mean ± SD.

See also Figure S1.

POLθ activity promotes gap filling at stalled replication forks

As POLθ accumulates at stalled forks containing ssDNA, its POL activity might contribute to lagging-strand synthesis under stressful conditions. To study the role of POLθ on normal and stalled forks, we used a POLθ polymerase inhibitor (POLθi) (Zatreanu et al., 2021) obtained from J. Loizou synthesized based on the structure of a recently published POLθi family (Blencowe et al., 2020a, 2020b) (Figure 3A) (see also accompanying manuscript). POLθi strongly inhibited *Xenopus* POLθ polymerase activity *in vitro* (Figure 3B). As POLθi did not impact on the overall levels of genomic DNA replication in egg extracts measured by bulk incorporation of α-^{32}PdCTP (Figure 3C), we verified whether it induced more subtle defects not detectable by this assay. To this end, we isolated RIs from interphase extracts treated with 5 μM POLθi and analyzed them by EM. Intriguingly, a significant fraction of RIs isolated from POLθi-treated extracts showed fork junction ssDNA gaps wider than the ones normally found on control RIs (Figures 3D and 3E). Accumulation of gaps of similar size was obtained by

these results, it is likely that the long uninterrupted ssDNA gaps observed with higher doses of APH are due to more effective inhibition of OKF formation and elongation, yielding dsDNA fragments too short to be cross-linked or visualized by EM, which has a resolution limit of ~40 nt. Asymmetric ssDNA accumulation induced by APH, which inhibits all replicative POLs, is likely explained by the fact that leading-strand synthesis by a single replisome proceeds for significantly longer tracts compared with the lagging strand (Graham et al., 2017). This configuration could be crystallized by APH-induced sudden arrest of all replicative POLs on individual molecules producing the RIs with asymmetric gaps observed by EM.

A

POLθi

B

C

a-³²P-dCTP

D POLθi

E

F

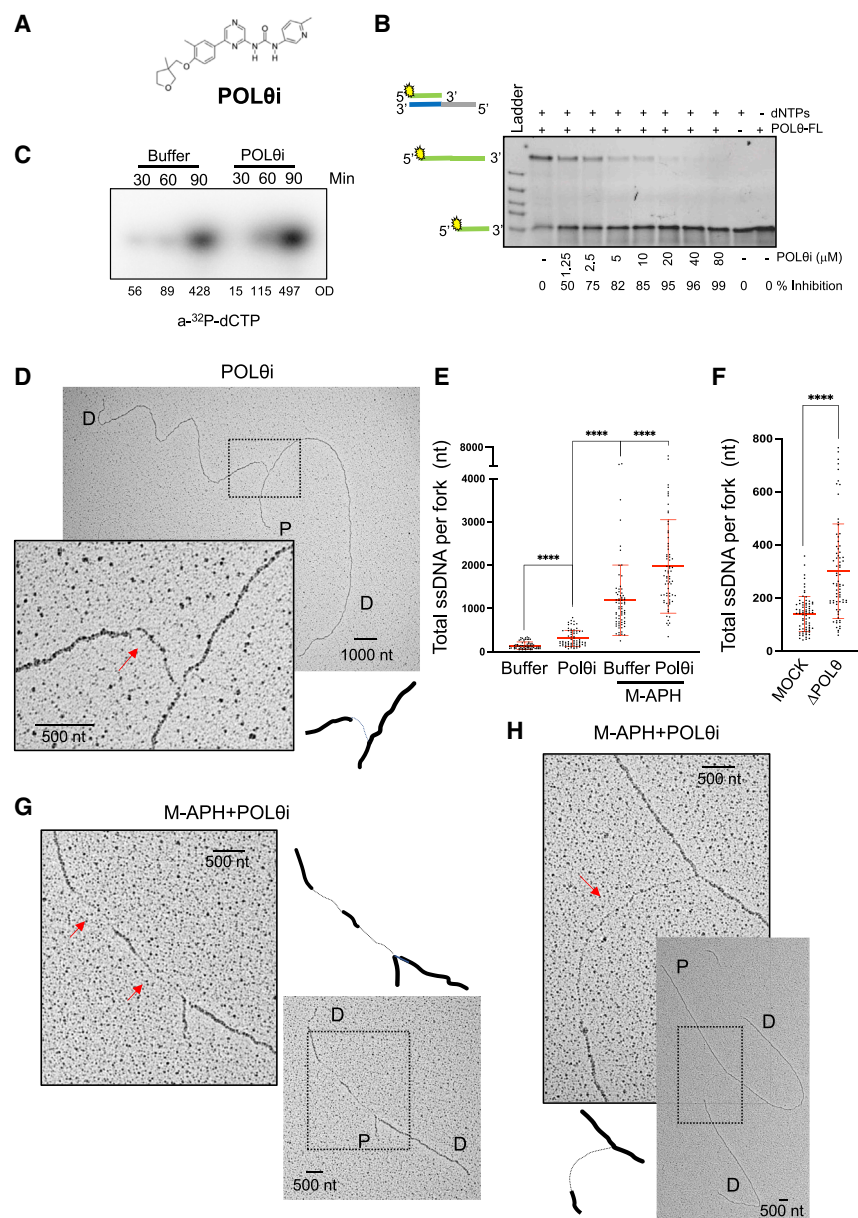**G** M-APH+POLθi

H M-APH+POLθi

Figure 3. POLθ polymerase inhibition impacts on replication fork ssDNA accumulation

(A) Chemical structure of POLθi.

(B) Representative denaturing gel showing POLθ-FL-mediated 3′-extension of a fluorescent DNA oligo in the presence of the indicated concentrations of POLθi. Percentage of DNA elongation inhibition is shown for each lane.

(C) Representative autoradiography showing incorporation of α-³²PdCTP in sperm nuclei incubated for the indicated times. ODs are indicated.

(D) Representative EM image of a replication fork isolated from an extract treated with POLθi (5 μM) for 60 min following sperm nuclei addition. Red arrow indicates ssDNA.

(E) Quantification of total ssDNA gap length for each replication fork represented in (D), (G), and (H) isolated from extracts treated with POLθi, M-APH, or both added 60 min after sperm nuclei addition and incubated for 45 min before DNA isolation. RIs were pooled from three independent experiments (n = 280); 70 RIs were counted for each treatment; horizontal bars indicate mean ± SD; unpaired t test; ***p < 0.001; ****p < 0.0001.

(F) Quantification of total ssDNA gap length for each fork isolated from mock or POLθ-depleted extracts. RIs were pooled from three independent experiments (n = 150); 75 RIs were counted for each treatment; horizontal bars indicate mean ± SD; unpaired t test; ****p < 0.0001.

(G and H) Representative EM images of replication forks isolated from an extract treated with POLθi and M-APH added 60 min after sperm nuclei addition and incubated for an additional 45 min before DNA isolation.

See also Figure S2.

depleting POLθ, indicating that the effect of POLθi was specific (Figure 3F).

We then induced fork stalling with M-APH and verified the effects of POLθi at fork junctions. Strikingly, the combination of M-APH and POLθi induced the accumulation of stalled OKFs with inter-OKF ssDNA gaps longer than M-APH alone, leading to a significant increase of the total amount of ssDNA accumulating at fork junctions (Figures 3E and 3G). In many cases, OKFs were no longer detectable resulting in uninterrupted long ssDNA at fork junctions (Figure 3H).

To further confirm that asymmetric ssDNA gaps derive from the stalling OKFs and that inhibition of POLθ impacts on them, we used CD437, a specific POLα inhibitor able to stall lagging-strand synthesis in cells (Han et al., 2016) and in *Xenopus* egg extracts (Ercilla et al., 2020). CD437 was able to

induce ssDNA gaps similar to the ones observed with APH (Figures S5A and S5B), which were extended by POLθi (Figures S5A and S5C) and inhibited by POLθ-FL overexpression (Figures S5A and S5D). CD437 also stimulated chromatin recruitment of POLθ and accumulation of RPA (Figure S5E). Moreover, Olaparib-mediated PARP1 inhibition, which prevents effective FEN1-dependent OKF maturation (Vaitsiankova et al., 2022), induced fork junction gaps (Figures S5A and S5F), the size of which was significantly increased by POLθ inhibition (Figures S5A and S5G) and decreased by POLθ-FL overexpression (Figures S5A and S5H).

Overall, these experiments indicate that gaps formed by OKF synthesis inhibition are major targets of POLθ, which prevents their accumulation by promoting stalled OKF elongation.

POLθ helicase and polymerase activities function in coordination to prevent ssDNA accumulation at replication forks

To further validate POLθ's role at stalled OKFs, we supplemented APH-treated extracts with an excess of active POLθ-FL,
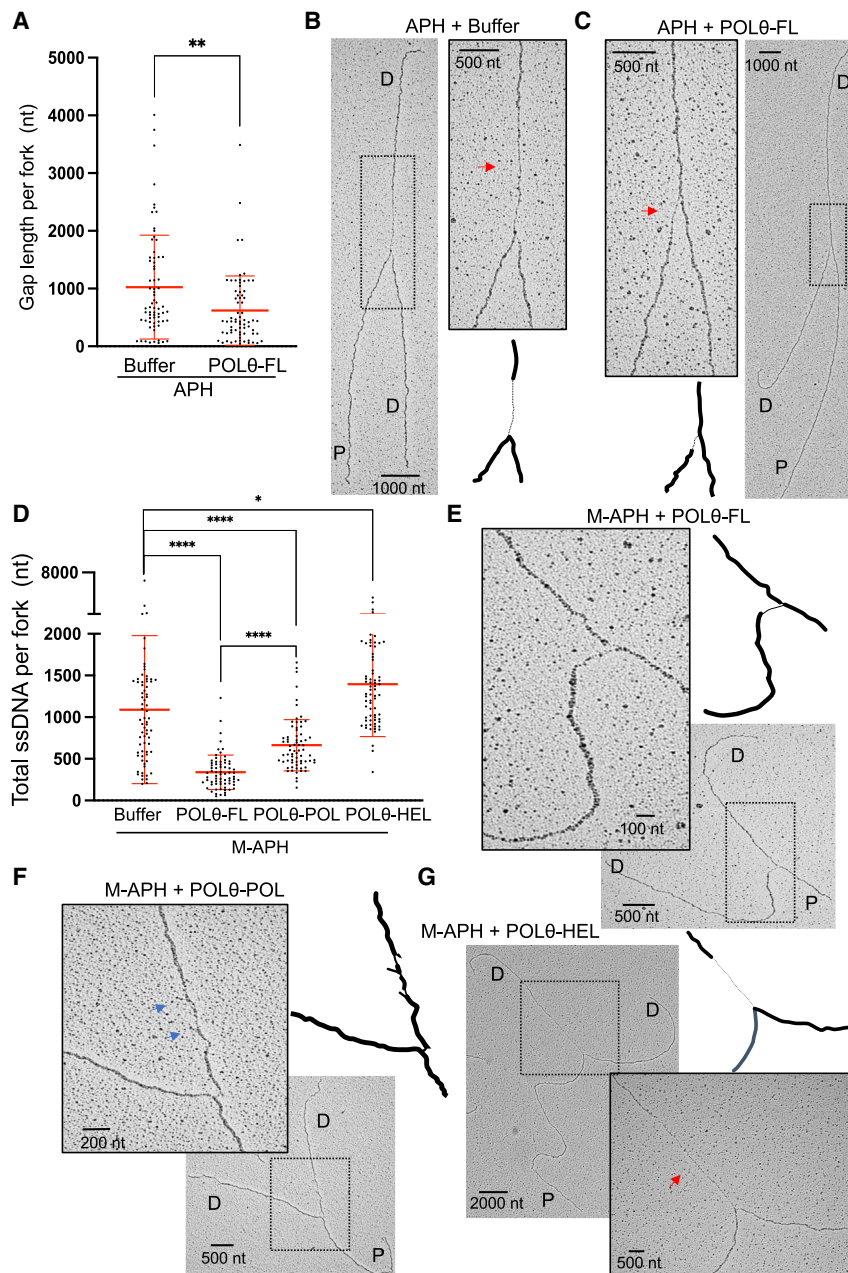
Figure 4. POLθ polymerase and helicase process stalled OKFs

(A) Quantification of fork junction ssDNA gap length for each replication fork isolated from extracts supplemented with buffer or POLθ-FL (25 nM) and treated with APH. Measurements were conducted on 150 RIs pooled from three independent experiments (n = 150); 75 RIs were counted for each treatment; horizontal bars indicate mean ± SD; unpaired t test; **p < 0.01.

(B and C) (B) Representative EM images of replication forks isolated from extracts supplemented buffer or (C) POLθ-FL and APH.

(D) Quantification of total ssDNA length for each replication fork represented in (E–G) isolated from extracts supplemented with buffer, POLθ-FL, POLθ-POL, or POLθ-HEL and treated with M-APH. RIs were pooled from three independent experiments (n = 280); 70 RIs were counted for each condition; horizontal bars indicate mean ± SD; unpaired t test; *p < 0.05; ****p < 0.0001.

(E–G) (E) EM images of replication forks isolated from extracts supplemented with POLθ-FL, (F) POLθ-POL (25 nM), or (G) POLθ-HEL treated with M-APH. Blue arrows indicate DNA flaps.

See also Figures S3–S5.

helicase domain is less proficient at preventing gaps between stalled OKFs in the presence of long flaps that could block the progression of other lagging-strand polymerases, including POLδ (Koc et al., 2015).

Overexpression of recombinant POLθ-HEL, instead, resulted in the removal of most stalled nascent OKFs, producing long stretches of ssDNA deprived of double-stranded DNA regions (Figure 4G) and leading to a further increase in the total ssDNA accumulation on each RI (Figure 4D).

These results suggest that POLθ uses its POL domain to fill the ssDNA gaps between the stalled OKFs and its helicase domain to remove secondary DNA structures or stalled OKFs that prevent an efficient POL function. Intriguingly, POLθ-FL-
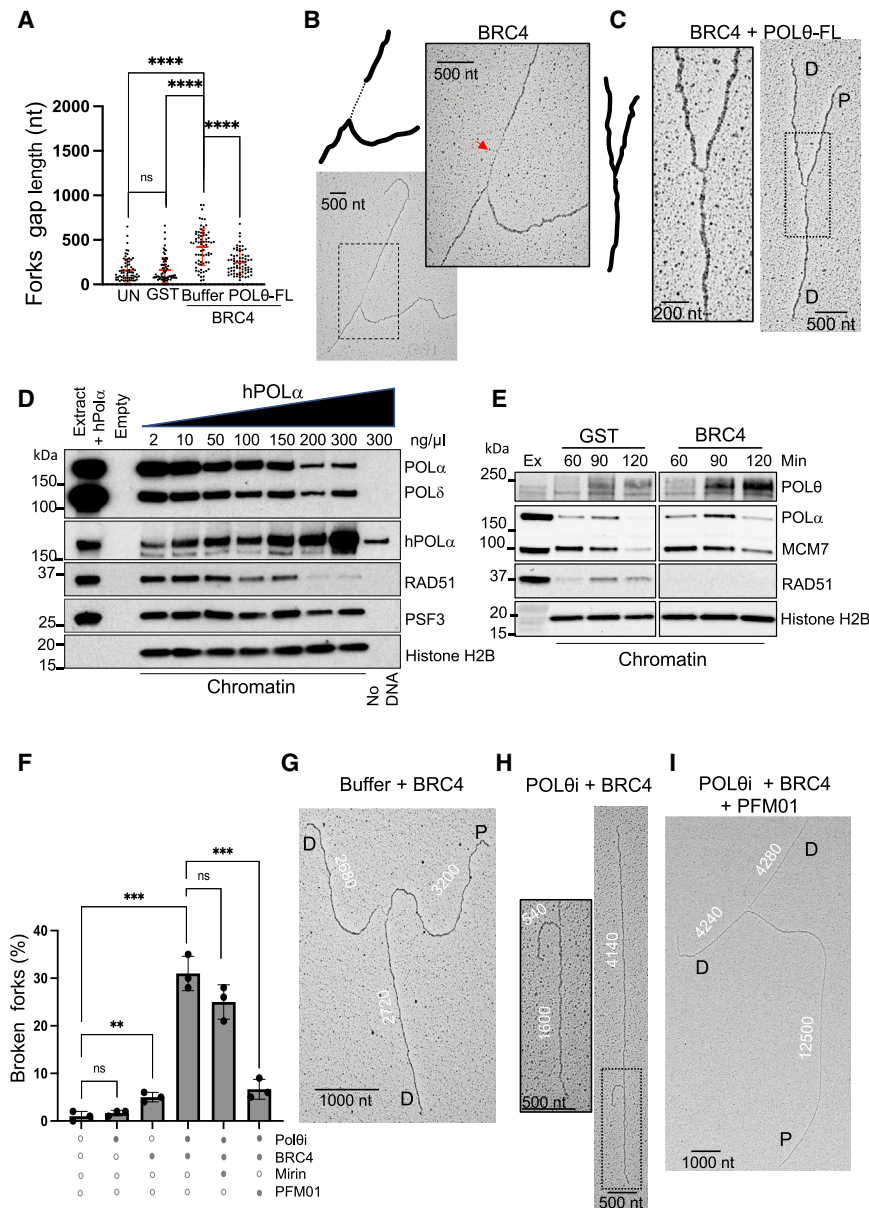
which was able to significantly reduce APH-induced and M-APH-induced gap size and number (Figures 4A–4C), decreasing total ssDNA accumulation on each RI (Figures 4C–4E). Under these conditions, individual OKFs could no longer be distinguished (Figure 4E), confirming that POLθ extended stalled OKFs filling ssDNA gaps between them.

Remarkably, an excess of recombinant POLθ-POL was less effective than POLθ-FL at suppressing gaps between OKFs, yielding partially filled intermediates, often containing 50 to 80-nt-long ssDNA flaps (Figure 4F). Consistently, POLθ-POL only partially reduced total ssDNA accumulation on each RI (Figure 4D). These results suggest that POLθ-POL lacking the

mediated suppression of ssDNA accumulation at fork junction strongly suppressed fork reversal induced by APH, consistent with ssDNA at forks being required for fork remodeling (Joseph et al., 2020; Poole and Cortez, 2017) (Figure S5I).

RAD51 and POLθ prevent the accumulation of ssDNA gaps on the lagging strand

To verify how the functional interaction between POLθ and HR proteins occurs during DNA replication, we studied the role of major HR protein RAD51 at fork junctions. In the absence of BRCA2 and/or RAD51 bound to chromatin, ssDNA gaps can form behind forks, due to the MRE11 exonuclease activity

Figure 5. POLθ and RAD51 bound to lagging-strand DNA protect stalled forks from MRE11-dependent cleavage

(A) Quantification of fork junction ssDNA gap length for each RI isolated from extracts that were treated as indicated. RIs pooled from three independent experiments (n = 300); 100 RIs were counted for each treatment; unpaired t test; ****p < 0.0001.

(B and C) (B) Representative EM images of replication forks isolated from extracts supplemented with GST-BRC4 (BRC4) or (C) GST-BRC4 and POLθ-FL.

(D) Representative WB showing the indicated proteins in extract or bound to chromatin isolated 60 min after addition of sperm nuclei to egg extracts supplemented with buffer or recombinant hPOLα complex at the indicated concentrations.

(E) Representative WB showing chromatin-binding time course of the indicated proteins in extracts that were treated with GST or GST-BRC4. Chromatin was isolated at the indicated times after sperm nuclei addition to interphase egg extracts. Rectangles delimitate relevant lanes derived from the same gel.

(F) Quantification of broken forks isolated from extracts supplemented with POLθi (5 μM), GST-BRC4 (0.4 mg/mL), 100 μM Mirin, or 100 μM PFM01 as indicated. RIs were pooled from independent experiments (n = 420); 70 RIs were counted for each treatment; columns indicate mean ± SD; unpaired t test; ***p < 0.001; ns, non-significant.

(G–I) (G) Representative EM images of replication forks isolated from extracts supplemented with GST-BRC4 and buffer, (H) GST-BRC4 and POLθi, or (I) GST-BRC4, POLθi, and PFM01. Numbers in white show the approximate length in nt for each DNA segment. Quantification for the representative images is shown in (F).

See also Figure S6.

toward nascent DNA. However, ssDNA gaps also form at fork junctions, independently of MRE11 exonuclease when RAD51 binding to DNA is prevented with a human-BRCA2-derived BRC4 peptide fused to glutathione-S-transferase (GST-BRC4 or BRC4), or, similarly, when RAD51 is immunodepleted (Hashimoto et al., 2010; Kolinjivadi et al., 2017b). Accordingly, GST-BRC4 added to egg extracts induced asymmetric fork junction gaps (Figures 5A and 5B), which were suppressed by POLθ-FL overexpression (Figures 5A and 5C).

To localize the gaps observed in the absence of RAD51 bound to DNA, the BRC4 peptide and APH were added to the same extract. The combination did not induce additional gaps on the opposite strand (Figure S6A), suggesting that similar to APH ssDNA accumulation observed in the absence of RAD51 bound to DNA occurs on the lagging strand.

We then performed a competition experiment with lagging-strand binding proteins to identify the strand engaged with RAD51. To this end, we supplemented egg extracts with an excess of recombinant human POLα primase (hPOLα) complex (Kolinjivadi et al., 2017b). Strikingly, hPOLα was able to replace endogenous POLα, the majority of which binds lagging-strand DNA (Pellegrini, 2012), outcompeting RAD51 chromatin binding (Figures 5D and S6B). These results suggest that a large fraction of RAD51 bound to replication forks is localized on lagging strands.

Significantly, inhibition of RAD51 binding to DNA strongly enhanced POLθ chromatin recruitment (Figures 5E and S6B), suggesting that also POLθ operates on lagging strands, possibly complementing RAD51 function.

POLθ prevents MRE11-mediated endo-nucleolytic fork cleavage in the absence of RAD51

We then asked what happens to replication forks when both POLθ and RAD51 are prevented from functioning. Strikingly,

while inhibition of RAD51 binding alone did not alter the integrity of daughter strands at forks (Figures 5F and 5G), inhibition of both POLθ polymerase and RAD51 DNA binding led to the accumulation of a significant number of RIs with all branches of different lengths (Figures 5F and 5H). Asymmetric RIs in which all three arms have different lengths could result from the endogenous cleavage of replication bubbles (Figure S6D), producing single-ended broken forks in RIs derived from extracts in which both POLθ polymerase and RAD51 are defective. This phenotype was especially evident on converging RIs containing one intact and one broken fork, respectively (Figures S6E and S6G).

To identify the molecular mechanisms leading to the formation of asymmetric RIs with broken arms, we tested the involvement of the MRE11 nuclease in strand cleavage (Paull, 2018). Strikingly, we found that the MRE11 endonuclease inhibitor PFM01 (Shibata et al., 2014) could efficiently prevent the formation of cleaved RIs induced by the combined inhibition of POLθ and RAD51 (Figures 5F, 5I, S6F, and S6G). Inhibiting MRE11 exonuclease activity with Mirin (Dupré et al., 2008) instead had a non-significant effect on the formation of broken RIs (Figure 5F). These results suggest that asymmetric RIs derive from MRE11-mediated endonucleolytic cleavage of lagging strand with unrepaired gaps formed in the absence of POLθ and RAD51. This activity would be compatible with MRE11 ability to cleave substrates containing ssDNA with a 5′-dsDNA junction mimicking lagging strands containing stalled OKFs (Deshpande et al., 2016).

POLθ prevents accumulation of ssDNA gaps and MRE11-dependent DSBs in BRCA2-defective cells

We then tested the effects of the POLθi on an isogenic pair of human colon cancer cell lines (DLD1) proficient or deficient for *BRCA2* (denoted DLD1 and DLD1 *BRCA2*$^{-/-}$, respectively). As previously reported (Zatreanu et al., 2021), POLθi induced DLD1 *BRCA2*$^{-/-}$ cell death (Figure S7A). To verify whether POLθ polymerase inhibition induced ssDNA gaps, we analyzed DNA fibers pulse-labeled with 5-chloro-2'-deoxyuridine (CldU) followed by IdU t mark ongoing replication forks. Before spreading DNA to obtain fibers, cells were permeabilized and treated with S1 nuclease, which cleaves DNA in the correspondence of ssDNA gaps (Quinet et al., 2017a; Tirman et al., 2021). S1 nuclease did not reduce the length of IdU tracks (Figure 6A), whereas POLθi treatment slightly shortened them in DLD1 cells (Figure 6B) probably due to fork speed reduction, as previously described (Ceccaldi et al., 2015) (Figures S7B and S7C). S1 nuclease in DLD1 BRCA2$^{-/-}$ cells, instead, reduced labeled fiber length, indicating increased ssDNA burden compared with the wild-type counterpart (Figure 6B). Strikingly, acute inhibition of POLθ POL with POLθi in DLD1 BRCA2$^{-/-}$ cells induced further S1-nuclease-dependent DNA fiber shortening compared with the same untreated cells (Figure 6B). The accumulation of ssDNA gaps in DLD1 *BRCA2*$^{-/-}$ cells was independent of MRE11 activities as it was neither suppressed by MRE11 exonuclease inhibitor Mirin (Figure 6B) or endonuclease inhibitor PFM01 (Figure S7D). POLθi-induced ssDNA accumulation during DNA replication was consistent with RPA foci accumulation in EdU-labeled DLD1 BRCA2$^{-/-}$ cells (Figures S7E and S7F). These results suggest that similar to what happen in *Xenopus*, BRCA2$^{-/-}$ cells sponta-

neously accumulate Mirin-insensitive ssDNA gaps during DNA replication that require POLθ to be filled.

Intriguingly, POLθ inhibition induced sporadic fork progression arrest compatible with fork collapse in DLD1 *BRCA2*$^{-/-}$ cells (Figure S7G). Accordingly, prolonged exposure to POLθi induced DSB accumulation in S-phase as shown by higher levels of phosphorylated histone H2AX (γH2AX) foci formation in DLD1 *BRCA2*$^{-/-}$ EdU-labeled cells compared to DLD1 cells (Figures S7H and S7I). Such DSBs were the product of asymmetric fork breakage and damage detected by EM (Figure 6C) on more than ∼80% of the RIs derived from DLD1 *BRCA2*$^{-/-}$ cells (Figure S7J). In contrast, the same alterations affected only ∼10% of the RIs derived from DLD1 cells (Figure S7J). Importantly, S-phase-associated DSBs could be prevented by the knockdown of MRE11, NBS1 (or NBN) or CtIP, which is required for MRE11 endonuclease activation (Figures 6D–6F). Similar results were obtained by inhibiting MRE11 endonuclease activity with PFM01 (Figures S7K and S7L).

We then verified the consequences of these knockdowns in DLD1 *BRCA2*$^{-/-}$ cells. Complete inactivation of MRE11 and NBS1/NBN core components of the MRN complex or of its modular subunit, CtIP, leads to cell death after few cell divisions (Chin and Villeneuve, 2001; Costanzo et al., 2004, 2001; Hashimoto et al., 2011; Makharashvili and Paull, 2015; Paull, 2018; Yamaguchi-Iwai et al., 1999). Therefore, complete inactivation of these genes is not expected to relieve possible cellular toxicity of POLθi-induced DSBs. However, we observed a consistent enhancement of the survival of DLD1 *BRCA2*$^{-/-}$ cells exposed to POLθi following the knockdown of the MRE11 endonuclease activator CtIP (Figure 6G), and a more limited, although reproducible, improvement induced by downregulation of MRE11 or NBS1/NBN expression over a short time (Figure 6G). These results suggest that decreased MRE11 endonuclease activity prevents, at least in part, the cytotoxicity induced by POLθi in BRCA2-defective cells by suppressing DSB accumulation.

DISCUSSION

Here, we describe a central role of POLθ in responding to stalled forks and promoting their stability in the absence of functional HR proteins. To summarize, we isolated *Xenopus* POLθ and showed that (1) POLθ can bind to replication forks, and its binding is enhanced by fork stalling; (2) stalled OKFs, induced by lagging-strand polymerases inhibition and directly visualized by EM, increase POLθ chromatin binding; (3) POLθ polymerase activity prevents ssDNA gap accumulation on lagging strands by extending stalled OKFs induced by POLα or PARP inhibition, whereas POLθ helicase activity removes stalled OKFs facilitating POLθ-mediated inter-OKFs gap filling; (4) POLθ chromatin recruitment is increased in the absence of RAD51; (5) POLθ-mediated processing of stalled OKFs prevents fork cleavage and consequent DSB formation induced by MRE11 endonuclease in the absence of functional BRCA2/RAD51 proteins; and (6) downregulation of CtIP expression, required to promote MRE11 endonuclease activity (Paull, 2018), partially suppresses the lethality induced by POLθ polymerase inhibition in BRCA2-defective cells. These
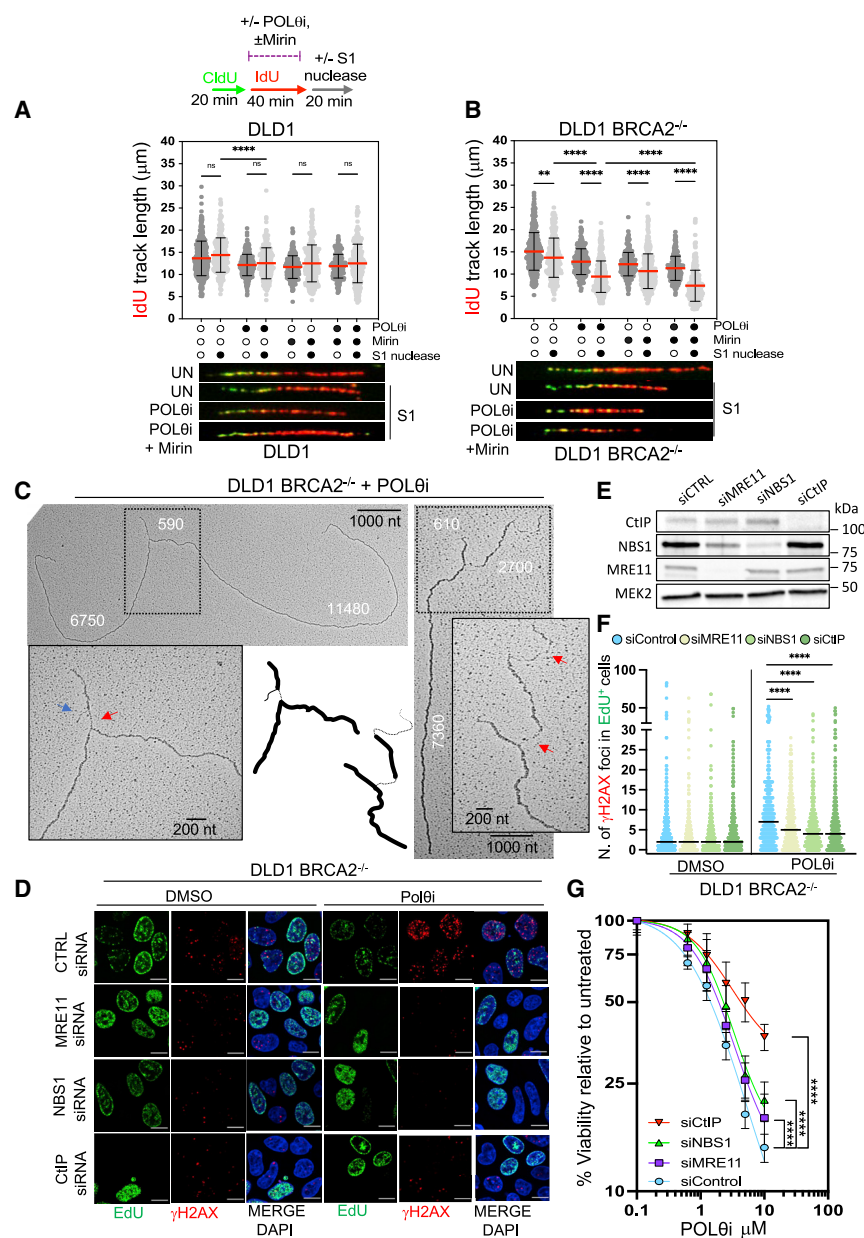
Figure 6. Inhibition of POLθ polymerase induces ssDNA gaps and MRE11-dependent DSB formation limiting BRCA2-defective cell survival

(A and B) (A) Schematic of the IdU/CldU pulse-labeling protocol followed by S1 nuclease treatment (top). Dot plot of IdU tract lengths (μm) in DLD1 cells or (B) DLD1 *BRCA2*$^{-/-}$ cells that were treated with DMSO (UN), 2 μM POLθi or 2 μM POLθi and 50 μM Mirin per experimental condition during the IdU pulse labeling. Horizontal bar indicates the mean. Kruskal-Wallis test; *p < 0.05, ***p < 0.001, ****p < 0.0001 (middle). Representative immunofluorescence images of labeled DNA fibers (bottom).

(C) Representative EM images of broken replication forks isolated from DLD1 *BRCA2*$^{-/-}$ cells treated with POLθi for 16 h. Numbers in white show the approximate length in nt for each DNA segment. Red arrows mark ssDNA gaps. Blue arrow marks DNA flaps.

(D) Representative confocal microscopy immunofluorescence of EdU-labeled DLD1 and DLD1 *BRCA2*$^{-/-}$ cells showing γH2AX foci (red) following siRNAs against the indicated targets and exposure to POLθi for 24 h. EdU-positive cells in green. DAPI staining in blue. Bars indicate 10 nm.

(E) Representative WB of the indicated proteins in DLD1 cells following siRNA-mediated knockdown.

(F) Dot plot of γH2AX foci number in EdU-labeled DLD1 *BRCA2*$^{-/-}$ cell nuclei as shown in (D); unpaired t test; **p < 0.01; ****p < 0.0001.

(G) Viability of DLD1 *BRCA2*$^{-/-}$ cells treated with increasing amounts of POLθi and the indicated siRNAs. Cell viability was assessed after 5 days, and it is expressed as a percentage of POLθi-treated viable cells relative to the untreated controls. Values represent the means ± SEMs of three independent biological replicates (n = 3); unpaired t test; ****p < 0.0001.

See also Figure S7.

results define a critical role of POLθ activities in promoting un-gapped DNA replication and preventing replication fork breakage in combination with HR proteins (Figures 7A–7F).

A major role of POLθ in ssDNA gap and DSB suppression during DNA replication

HR-defective cells exhibit an abnormal accumulation of ssDNA gaps, a phenomenon we originally observed during DNA replication in the absence of RAD51 bound to DNA and subsequently confirmed under BRCA1/2-defective conditions (Cantor, 2021; Chen et al., 2018; Feng and Jasin, 2017; Hashimoto et al., 2010; Kolinjivadi et al., 2017b; Taglialatela et al., 2017, 2021). These results indicate an essential role of HR proteins in suppressing replication-associated gaps.

Persistent ssDNA gaps formed during DNA replication have been linked to genotoxic agent-induced cell killing (Cong and Cantor, 2022), which is increased in the absence of gap filling trans-lesion POLs (TLSPs) (Taglialatela et al., 2021).

Here, we show that POLθ can process and suppress gaps induced by lagging-strand replication impairment following POLα or PARP1 inhibition, which impacts on OKF maturation (Hanzlikova et al., 2018; Vaitsiankova et al., 2022). This function of POLθ is important to prevent DSB accumulation.

POLθ promotes alt-NHEJ at DSBs with microhomology, a function essential to repair chromosome breakage in the absence of functional HR (Brambati et al., 2020; Ceccaldi et al., 2015; Higgins and Boulton, 2018; Mateos-Gomez et al., 2015; Schrempf et al., 2021; Wood and Doublié, 2016). POLθ-dependent alt-NEHJ is exploited by tumors with defective HR, in which overexpression POLθ complements defective HR-mediated DSB repair.
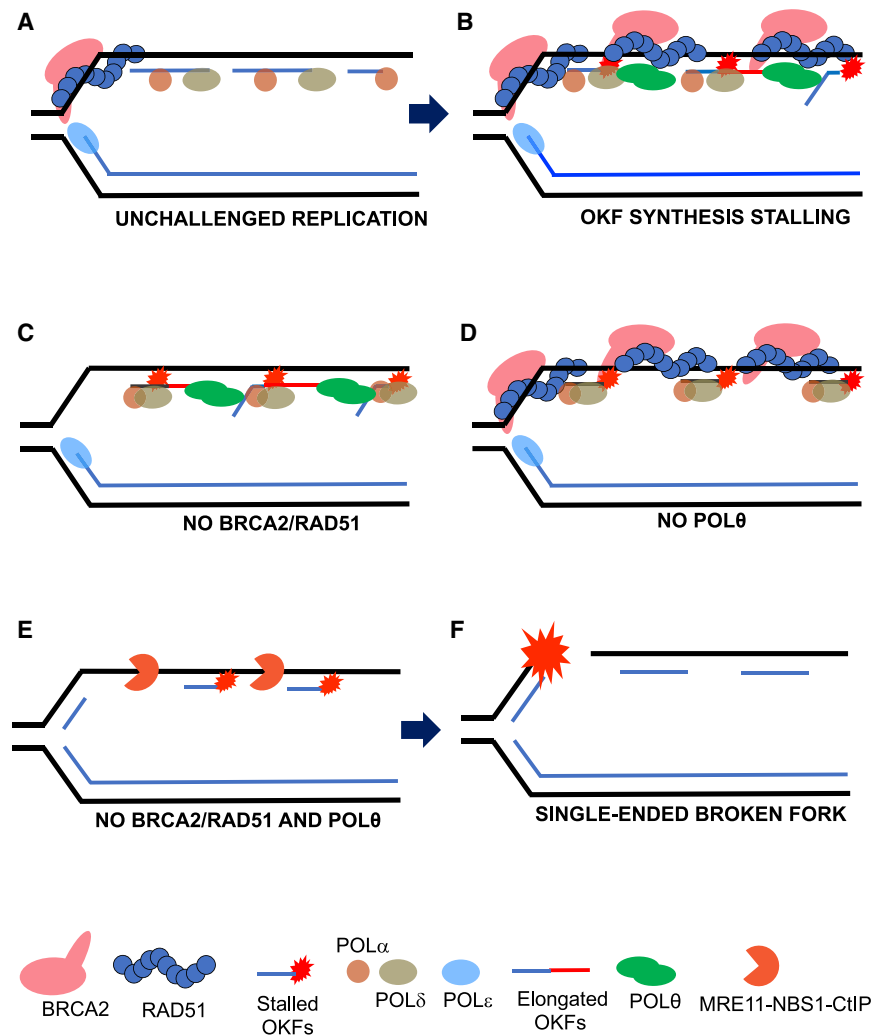
Figure 7. Proposed model for RAD51- and POLθ-mediated fork protection from MRE11 endonuclease

(A) BRCA2/RAD51 dynamically associates to replication forks, protecting ssDNA emerging from parental dsDNA unwinding and facilitating POLα/POLδ-mediated lagging-strand DNA synthesis.

(B) OKF stalling and ssDNA accumulation stimulate POLθ and BRCA2/RAD51 recruitment onto chromatin to process OKFs. POLθ polymerase extends OKFs, whereas POLθ helicase displaces 5′-flaps containing OKFs.

(C) Without BRCA2/RAD51, ssDNA accumulates attracting POLθ, which fills inter-OKF gaps.

(D) In the absence of POLθ, BRCA2/RAD51 binding to chromatin is sufficient to protect ssDNA.

(E) In the absence of both POLθ and BRCA2/RAD51, the MRE11-NBS1/NBN-CtIP endonuclease gains access to gapped forks.

(F) The MRE11-NBS1/NBN-CtIP endonuclease cleaves DNA producing broken forks.

highlighted a role of POLθ-FL in processing stalled OKFs. Secondary DNA structures, RNA-DNA hybrids or long 5′-flaps that can halt POLδ progression (Koc et al., 2015), can be displaced by POLθ helicase (Ozdemir et al., 2018). Accordingly, overexpression of POLθ-HEL removes stalled OKFs on endogenous forks, and POLθ-FL polymerizes DNA past an annealed oligo *in vitro*. In contrast, helicase-defective POLθ-POL is unable to bypass OKFs containing long flaps in egg extracts, yielding instead partially filled RIs. As the bypass observed *in vitro* with POLθ-FL is not complete compared to egg extracts, additional factors present at stalled forks or post-translational modifications might be required to stimulate POLθ-FL activities.

Previous work also found POLθ at replication origins where it might regulate replication onset and respond to replication stress (Fernandez-Vidal et al., 2014; Lemée et al., 2010). POLθ might facilitate the bypass of endogenous DNA lesions caused by spontaneous base depurination, deamination, or oxidation leading to the formation of abasic sites, like the ones produced by base excision repair (BER) DNA glycosylase SMUG1 (Taglialatela et al., 2021). This would be compatible with the ability of POLθ to replicate over ssDNA templates containing apurinic and apyrimidinic sites (Hogg et al., 2011).

A role of POLθ on lagging strands could explain the importance of POLθ in the absence of BRCA1/2 and RAD51 bound to replicating DNA. Previous results have shown that BRCA2 and RAD51 prevent MRE11-indepedent gaps occurring only on side at fork junctions and MRE11-dependent gaps arising behind forks away from fork junctions on both strands (Hashimoto et al., 2010; Kolinjivadi et al., 2017b). At fork junctions, BRCA2/RAD51 might bind to ssDNA exposed on the lagging strand, as suggested by our observation that POLα

Our results indicate that in addition to repairing DSBs, POLθ also prevents their formation by protecting replication forks from breakage. This function might limit DSB accumulation in HR-deficient, and, to some extent, HR-proficient cells, explaining synthetic sickness produced by the loss of POLθ and either HR- (Brambati et al., 2020; Ceccaldi et al., 2015; Mateos-Gomez et al., 2015) or NHEJ-dependent DSBs repair (Wyatt et al., 2016; Zatreanu et al., 2021). Understanding how gap-filling-dependent DNA breakage prevention is coordinated with HR-dependent and -independent DSB repair pathways will require further studies.

Surprisingly, reversed forks bearing a DNA end are not required to load POLθ onto chromatin. Instead, POLθ-mediated gap filling inhibits fork reversal by suppressing ssDNA-containing intermediates required for fork remodeling, similar to what was previously reported (Joseph et al., 2020; Poole and Cortez, 2017).

POLθ and HR proteins interplay at replication forks

In vitro studies have assigned diverse functions to POLθ domains (Black et al., 2016; Brambati et al., 2020; Ozdemir et al., 2018; Wood and Doublié, 2016). The *Xenopus* cell-free extract

overexpression outcompetes and displaces RAD51 from repli-cating chromatin. A shorter DNA-binding site of RAD51, which occupies only 3 nt (Qiu et al., 2013), might facilitate dynamic engagement of several RAD51 molecules with inter-OKFs ssDNA. Once loaded, RAD51 could promote POLα-mediated OKF synthesis (Kolinjivadi et al., 2017b). Alternatively, BRCA2/RAD51 bound to lagging strands could reach out for replisome components on the leading strands such as MCM10, restraining fork progression (Kang et al., 2021), thus recoupling leading and lagging-strand synthesis.

Increased loading of POLθ onto chromatin in the absence of RAD51 and ineffective suppression of POLθi-induced gaps by MRE11 inhibition are consistent with lagging strands being a target for POLθ in HR-defective cells although an additional role of POLθ on leading strands cannot be excluded. However, as POLθ helicase activity would be dispensable in the absence of stalled OKFs, other polymerases, including PrimPol, could play a more important function on the leading strand, especially following DNA damage. Intriguingly, PrimPol has recently been shown to act primarily on leading strands even when lagging-strand synthesis is impaired (Mehta et al., 2022).

RAD51- and POLθ-mediated suppression of MRE11-dependent fork cleavage

MRE11 endonuclease can cleave ssDNA regions containing dsDNA, especially in the presence of proteins stably bound at the 5′- or 3′- ends of the same molecule, a substrate resembling stalled OKFs with stably bound blocked polymerases. This activity is strongly stimulated by CtIP during S-phase (Anand et al., 2016; Paull, 2018; Williams et al., 2009). ssDNA accumulating at forks in the absence of POLθ and BRCA2/RAD51 is exposed to the attack of nucleases, including the MRE11 complex, producing single-ended forks observed by EM. Fork breakage in S-phase produces the DSBs detected in HR-defective cells following POLθ inhibition and can be restrained by inhibition of MRE11 endonuclease.

Cleavage of stalled forks by MRE11 and other lagging-strand nucleases (Kim et al., 2017) in POLθ-proficient cells might help to resolve irreversible fork stalling, promoting cell survival. Accordingly, the loss of the MRE11 nuclease inhibitor DYNLL1 confers survival advantage to HR-defective cells (He et al., 2018). POLθ might be well placed on lagging strands not only to prevent fork breakage but also to recapture the broken ends and promote fork repair.

As POLθ inhibition is considered to be an anticancer strategy to kill HR-defective tumors (Higgins and Boulton, 2018; Schrempf et al., 2021; Zatreanu et al., 2021; Zhou et al., 2021), further studies are warranted to assess whether nonlethal cancer mutations in Mre11-Nbs1/Nbn-CtIP genes (Bogdanova et al., 2008; Park et al., 2011; Zarrizi et al., 2020) render HR-defective cancer cells resistant to POLθ inhibitors.

Limitations of the study

Here, we report an increase in ssDNA gaps upon POLθ inhibition in RAD51- and BRCA2-deficient backgrounds predisposing to MRE11 endonuclease-dependent fork breakage. Although we could clearly observe POLθi-induced HR-defective cell lethality, we could not determine whether the survival impairment is exclu-sively due to DSB formation in S- or other cell cycle phases. This is due to the additional essential roles played by the MRE11 complex, inactivation of which could not completely suppress POLθi-induced lethality. We could therefore not exclude that HR-impaired cell survival defects arise directly from the accumulation of ssDNA gaps, which could elicit other types of cytotoxic events, including the formation of aberrant DNA repair intermediates. Further investigations relying on the isolation of separation of function mutations in these genes will be required to address this point.

STAR★METHODS

Detailed methods are provided in the online version of this paper and include the following:

- KEY RESOURCES TABLE
- RESOURCE AVAILABILITY
  ○ Lead Contact
  ○ Materials Availability
  ○ Data and code availability
- EXPERIMENTAL MODEL AND SUBJECT DETAILS
  ○ *Xenopus laevis* eggs
  ○ Cell culture
- METHOD DETAILS
  ○ DNA constructs
  ○ Protein expression and purification
  ○ Antibody production
  ○ OLIGO extension assay and GAP-filling
  ○ Egg extract and chromatin binding
  ○ DNA Electron microscopy
  ○ Depletions
  ○ IPOND
  ○ RNA Interference
  ○ Immunofluorescence
  ○ DNA fiber analysis
  ○ S1 assay
  ○ Cell viability assay
  ○ Reagents
  ○ Antibodies
  ○ Software Availability
- QUANTIFICATION AND STATISTICAL ANALYSIS
  ○ Statistical analysis

REFERENCES

Anand, R., Ranjha, L., Cannavo, E., and Cejka, P. (2016). Phosphorylated CtIP functions as a co-factor of the MRE11-RAD50-NBS1 endonuclease in DNA end resection. Mol. Cell 64, 940–950. https://doi.org/10.1016/j.molcel.2016.10.017.

Aze, A., Sannino, V., Soffientini, P., Bachi, A., and Costanzo, V. (2016). Centromeric DNA replication reconstitution reveals DNA loops and ATR checkpoint suppression. Nat. Cell Biol. 18, 684–691. https://doi.org/10.1038/ncb3344.

Black, S.J., Kashkina, E., Kent, T., and Pomerantz, R.T. (2016). DNA polymerase theta: a unique multifunctional end-joining machine. Genes (Basel) 7, 67. https://doi.org/10.3390/genes7090067.

Blencowe, P., Charles, M., Cridland, A., Edkwuru, T., Heald, R., Macdonald, E., et al. (2020a). Heterocyclic substituted ureas, for use against cancer. World patent WO/2020/030925.

Blencowe, P., Charles, M., Cridland, A., Edkwuru, T., Heald, R., Macdonald, E., et al. (2020b). Thiazolureas as anticancer agents. World patent WO/2020/030924.

Bogdanova, N., Feshchenko, S., Schürmann, P., Waltes, R., Wieland, B., Hillemanns, P., Rogov, Y.I., Dammann, O., Bremer, M., Karstens, J.H., et al. (2008). Nijmegen breakage syndrome mutations and risk of breast cancer. Int. J. Cancer 122, 802–806. https://doi.org/10.1002/ijc.23168.

Brambati, A., Barry, R.M., and Sfeir, A. (2020). DNA polymerase theta (Polθ) – an error-prone polymerase necessary for genome stability. Curr. Opin. Genet. Dev. 60, 119–126. https://doi.org/10.1016/j.gde.2020.02.017.

Cantor, S.B. (2021). Revisiting the BRCA-pathway through the lens of replication gap suppression: "Gaps determine therapy response in BRCA mutant cancer". DNA Repair 107, 103209. https://doi.org/10.1016/j.dnarep.2021.103209.

Ceccaldi, R., Liu, J.C., Amunugama, R., Hajdu, I., Primack, B., Petalcorin, M.I.R., O'Connor, K.W., Konstantinopoulos, P.A., Elledge, S.J., Boulton, S.J., et al. (2015). Homologous-recombination-deficient tumours are dependent on Polθ-mediated repair. Nature 518, 258–262. https://doi.org/10.1038/nature14184.

Cech, T.R., Potter, D., and Pardue, M.L. (1978). Chromatin structure in living cells. Cold Spring Harb. Symp. Quant. Biol. 42, 191–198. https://doi.org/10.1101/sqb.1978.042.01.021.

Challberg, M.D., and Englund, P.T. (1980). Specific labeling of 3′ termini with T4 DNA polymerase. Methods Enzymol. 65, 39–43. https://doi.org/10.1016/s0076-6879(80)65008-3.

Chang, H.H.Y., Pannunzio, N.R., Adachi, N., and Lieber, M.R. (2017). Non-homologous DNA end joining and alternative pathways to double-strand break repair. Nat. Rev. Mol. Cell Biol. 18, 495–506. https://doi.org/10.1038/nrm.2017.48.

Chen, C.C., Feng, W., Lim, P.X., Kass, E.M., and Jasin, M. (2018). Homology-directed repair and the role of BRCA1, BRCA2, and related proteins in genome integrity and cancer. Annu. Rev. Cancer Biol. 2, 313–336. https://doi.org/10.1146/annurev-cancerbio-030617-050502.

Chin, G.M., and Villeneuve, A.M. (2001). C. elegans mre-11 is required for meiotic recombination and DNA repair but is dispensable for the meiotic G(2) DNA damage checkpoint. Genes Dev. 15, 522–534. https://doi.org/10.1101/gad.864101.

Cong, K., and Cantor, S.B. (2022). Exploiting replication gaps for cancer therapy. Mol. Cell 82, 2363–2369. https://doi.org/10.1016/j.molcel.2022.04.023.

Cong, K., Peng, M., Kousholt, A.N., Lee, W.T.C., Lee, S., Nayak, S., Krais, J., VanderVere-Carozza, P.S., Pawelczak, K.S., Calvo, J., et al. (2021). Replication gaps are a key determinant of PARP inhibitor synthetic lethality with BRCA deficiency. Mol. Cell 81, 3227. https://doi.org/10.1016/j.molcel.2021.07.015.

Costanzo, V., and Gautier, J. (2004). Xenopus cell-free extracts to study DNA damage checkpoints. Methods Mol. Biol. 241, 255–267.

Costanzo, V., Paull, T., Gottesman, M., and Gautier, J. (2004). Mre11 assembles linear DNA fragments into DNA damage signaling complexes. PLoS Biol. 2, E110. https://doi.org/10.1371/journal.pbio.0020110.

Costanzo, V., Robertson, K., Bibikova, M., Kim, E., Grieco, D., Gottesman, M., Carroll, D., and Gautier, J. (2001). Mre11 protein complex prevents double-strand break accumulation during chromosomal DNA replication. Mol. Cell 8, 137–147. https://doi.org/10.1016/s1097-2765(01)00294-5.

Deshpande, R.A., Lee, J.H., Arora, S., and Paull, T.T. (2016). Nbs1 converts the human Mre11/Rad50 nuclease complex into an endo/exonuclease machine specific for protein-DNA adducts. Mol. Cell 64, 593–606. https://doi.org/10.1016/j.molcel.2016.10.010.

Dungrawala, H., and Cortez, D. (2015). Purification of proteins on newly synthesized DNA using iPOND. Methods Mol. Biol. 1228, 123–131. https://doi.org/10.1007/978-1-4939-1680-1_10.

Dupré, A., Boyer-Chatenet, L., Sattler, R.M., Modi, A.P., Lee, J.H., Nicolette, M.L., Kopelovich, L., Jasin, M., Baer, R., Paull, T.T., and Gautier, J. (2008). A forward chemical genetic screen reveals an inhibitor of the Mre11-Rad50-Nbs1 complex. Nat. Chem. Biol. 4, 119–125. https://doi.org/10.1038/nchembio.63.

Ercilla, A., Benada, J., Amitash, S., Zonderland, G., Baldi, G., Somyajit, K., Ochs, F., Costanzo, V., Lukas, J., and Toledo, L. (2020). Physiological tolerance to ssDNA enables strand uncoupling during DNA replication. Cell Rep. 30, 2416.e7. 2429.e7. https://doi.org/10.1016/j.celrep.2020.01.067.

Feng, W., and Jasin, M. (2017). BRCA2 suppresses replication stress-induced mitotic and G1 abnormalities through homologous recombination. Nat. Commun. 8, 525. https://doi.org/10.1038/s41467-017-00634-0.

Fernandez-Vidal, A., Guitton-Sert, L., Cadoret, J.C., Drac, M., Schwob, E., Baldacci, G., Cazaux, C., and Hoffmann, J.S. (2014). A role for DNA polymerase θ in the timing of DNA replication. Nat. Commun. 5, 4285. https://doi.org/10.1038/ncomms5285.

Graham, J.E., Marians, K.J., and Kowalczykowski, S.C. (2017). Independent and stochastic action of DNA polymerases in the replisome. Cell 169, 1201.e17. 1213.e17. https://doi.org/10.1016/j.cell.2017.05.041.

Han, T., Goralski, M., Capota, E., Padrick, S.B., Kim, J., Xie, Y., and Nijhawan, D. (2016). The antitumor toxin CD437 is a direct inhibitor of DNA polymerase α. Nat. Chem. Biol. 12, 511–515. https://doi.org/10.1038/nchembio.2082.

Hanzlikova, H., Kalasova, I., Demin, A.A., Pennicott, L.E., Cihlarova, Z., and Caldecott, K.W. (2018). The importance of poly(ADP-ribose) polymerase as a sensor of unligated Okazaki fragments during DNA replication. Mol. Cell 71, 319.e3. 331.e3. https://doi.org/10.1016/j.molcel.2018.06.004.

Hashimoto, Y., and Costanzo, V. (2011). Studying DNA replication fork stability in Xenopus egg extract. Methods Mol. Biol. *745*, 437–445. https://doi.org/10.1007/978-1-61779-129-1_25.

Hashimoto, Y., Puddu, F., and Costanzo, V. (2011). RAD51- and MRE11-dependent reassembly of uncoupled CMG helicase complex at collapsed replication forks. Nat. Struct. Mol. Biol. *19*, 17–24. https://doi.org/10.1038/nsmb.2177.

Hashimoto, Y., Ray Chaudhuri, A., Lopes, M., and Costanzo, V. (2010). Rad51 protects nascent DNA from Mre11-dependent degradation and promotes continuous DNA synthesis. Nat. Struct. Mol. Biol. *17*, 1305–1311. https://doi.org/10.1038/nsmb.1927.

He, Y.J., Meghani, K., Caron, M.C., Yang, C., Ronato, D.A., Bian, J., Sharma, A., Moore, J., Niraj, J., Detappe, A., et al. (2018). DYNLL1 binds to MRE11 to limit DNA end resection in BRCA1-deficient cells. Nature *563*, 522–526. https://doi.org/10.1038/s41586-018-0670-5.

Higgins, G.S., and Boulton, S.J. (2018). Beyond PARP-POLθ as an anticancer target. Science *359*, 1217–1218. https://doi.org/10.1126/science.aar5149.

Hogg, M., Seki, M., Wood, R.D., Doublié, S., and Wallace, S.S. (2011). Lesion bypass activity of DNA polymerase θ(POLQ) is an intrinsic property of the pol domain and depends on unique sequence inserts. J. Mol. Biol. *405*, 642–652. https://doi.org/10.1016/j.jmb.2010.10.041.

Joseph, S.A., Taglialatela, A., Leuzzi, G., Huang, J.W., Cuella-Martin, R., and Ciccia, A. (2020). Time for remodeling: SNF2-family DNA translocases in replication fork metabolism and human disease. DNA Repair *95*, 102943. https://doi.org/10.1016/j.dnarep.2020.102943.

Kang, Z., Fu, P., Alcivar, A.L., Fu, H., Redon, C., Foo, T.K., Zuo, Y., Ye, C., Baxley, R., Madireddy, A., et al. (2021). BRCA2 associates with MCM10 to suppress PRIMPOL-mediated repriming and single-stranded gap formation after DNA damage. Nat. Commun. *12*, 5966. https://doi.org/10.1038/s41467-021-26227-6.

Kim, H.S., Nickoloff, J.A., Wu, Y., Williamson, E.A., Sidhu, G.S., Reinert, B.L., Jaiswal, A.S., Srinivasan, G., Patel, B., Kong, K., et al. (2017). Endonuclease EEPD1 is a gatekeeper for repair of stressed replication forks. J. Biol. Chem. *292*, 2795–2804. https://doi.org/10.1074/jbc.M116.758235.

Koc, K.N., Stodola, J.L., Burgers, P.M., and Galletto, R. (2015). Regulation of yeast DNA polymerase delta-mediated strand displacement synthesis by 5′-flaps. Nucleic Acids Res. *43*, 4179–4190. https://doi.org/10.1093/nar/gkv260.

Kolinjivadi, A.M., Sannino, V., de Antoni, A., Técher, H., Baldi, G., and Costanzo, V. (2017a). Moonlighting at replication forks - a new life for homologous recombination proteins BRCA1, BRCA2 and RAD51. FEBS Lett. *591*, 1083–1100. https://doi.org/10.1002/1873-3468.12556.

Kolinjivadi, A.M., Sannino, V., De Antoni, A., Zadorozhny, K., Kilkenny, M., Técher, H., Baldi, G., Shen, R., Ciccia, A., Pellegrini, L., et al. (2017b). Smarcal1-mediated fork reversal triggers Mre11-dependent degradation of nascent DNA in the absence of BRCA2 and stable Rad51 nucleofilaments. Mol. Cell *67*, 867.e7. 881.e7. https://doi.org/10.1016/j.molcel.2017.07.001.

Lemée, F., Bergoglio, V., Fernandez-Vidal, A., Machado-Silva, A., Pillaire, M.J., Bieth, A., Gentil, C., Baker, L., Martin, A.L., Leduc, C., et al. (2010). DNA polymerase theta up-regulation is associated with poor survival in breast cancer, perturbs DNA replication, and promotes genetic instability. Proc. Natl. Acad. Sci. USA *107*, 13390–13395. https://doi.org/10.1073/pnas.0910759107.

Makharashvili, N., and Paull, T.T. (2015). CtIP: a DNA damage response protein at the intersection of DNA metabolism. DNA Repair *32*, 75–81. https://doi.org/10.1016/j.dnarep.2015.04.016.

Mateos-Gomez, P.A., Gong, F., Nair, N., Miller, K.M., Lazzerini-Denchi, E., and Sfeir, A. (2015). Mammalian polymerase θ promotes alternative NHEJ and suppresses recombination. Nature *518*, 254–257. https://doi.org/10.1038/nature14157.

McGarry, T.J., and Kirschner, M.W. (1998). Geminin, an inhibitor of DNA replication, is degraded during mitosis. Cell *93*, 1043–1053. https://doi.org/10.1016/s0092-8674(00)81209-x.

Mehta, K.P.M., Thada, V., Zhao, R., Krishnamoorthy, A., Leser, M., Lindsey Rose, K., and Cortez, D. (2022). CHK1 phosphorylates PRIMPOL to promote replication stress tolerance. Sci. Adv. *8*, eabm0314. https://doi.org/10.1126/sciadv.abm0314.

Ozdemir, A.Y., Rusanov, T., Kent, T., Siddique, L.A., and Pomerantz, R.T. (2018). Polymerase θ-helicase efficiently unwinds DNA and RNA-DNA hybrids. J. Biol. Chem. *293*, 5259–5269. https://doi.org/10.1074/jbc.RA117.000565.

Panzarino, N.J., Krais, J.J., Cong, K., Peng, M., Mosqueda, M., Nayak, S.U., Bond, S.M., Calvo, J.A., Doshi, M.B., Bere, M., et al. (2021). Replication gaps underlie BRCA deficiency and therapy response. Cancer Res. *81*, 1388–1397. https://doi.org/10.1158/0008-5472.CAN-20-160.

Park, Y.B., Chae, J., Kim, Y.C., and Cho, Y. (2011). Crystal structure of human Mre11: understanding tumorigenic mutations. Structure *19*, 1591–1602. https://doi.org/10.1016/j.str.2011.09.010.

Paull, T.T. (2018). 20 years of Mre11 biology: no end in sight. Mol. Cell *71*, 419–427. https://doi.org/10.1016/j.molcel.2018.06.033.

Pellegrini, L. (2012). The Pol alpha-primase complex. Subcell. Biochem. *62*, 157–169. https://doi.org/10.1007/978-94-007-4572-8_9.

Poole, L.A., and Cortez, D. (2017). Functions of SMARCAL1, ZRANB3, and HLTF in maintaining genome stability. Crit. Rev. Biochem. Mol. Biol. *52*, 696–714. https://doi.org/10.1080/10409238.2017.1380597.

Qiu, Y., Antony, E., Doganay, S., Koh, H.R., Lohman, T.M., and Myong, S. (2013). Srs2 prevents Rad51 filament formation by repetitive motion on DNA. Nat. Commun. *4*, 2281. https://doi.org/10.1038/ncomms3281.

Quinet, A., Carvajal-Maldonado, D., Lemacon, D., and Vindigni, A. (2017a). DNA fiber analysis: mind the gap! Methods Enzymol. *591*, 55–82. https://doi.org/10.1016/bs.mie.2017.03.019.

Quinet, A., Lemaçon, D., and Vindigni, A. (2017b). Replication fork reversal: players and guardians. Mol. Cell *68*, 830–833. https://doi.org/10.1016/j.molcel.2017.11.022.

Quinet, A., Tirman, S., Jackson, J., Šviković, S., Lemaçon, D., Carvajal-Maldonado, D., González-Acosta, D., Vessoni, A.T., Cybulla, E., Wood, M., et al. (2020). PRIMPOL-mediated adaptive response suppresses replication fork reversal in BRCA-deficient cells. Mol. Cell *77*, 461.e9. 474.e9. https://doi.org/10.1016/j.molcel.2019.10.008.

Raspelli, E., Falbo, L., and Costanzo, V. (2017). *Xenopus* egg extract to study regulation of genome-wide and locus-specific DNA replication. Genesis *55*. https://doi.org/10.1002/dvg.22996.

Sannino, V., Kolinjivadi, A.M., Baldi, G., and Costanzo, V. (2016). Studying essential DNA metabolism proteins in Xenopus egg extract. Int. J. Dev. Biol. *60*, 221–227. https://doi.org/10.1387/ijdb.160103vc.

Sannino, V., Pezzimenti, F., Bertora, S., and Costanzo, V. (2017). *Xenopus laevis* as model system to study DNA damage response and replication fork stability. Methods Enzymol. *591*, 211–232. https://doi.org/10.1016/bs.mie.2017.03.018.

Schrempf, A., Slyskova, J., and Loizou, J.I. (2021). Targeting the DNA repair enzyme polymerase θ in cancer therapy. Trends Cancer *7*, 98–111. https://doi.org/10.1016/j.trecan.2020.09.007.

Seki, M., Marini, F., and Wood, R.D. (2003). POLQ (Pol theta), a DNA polymerase and DNA-dependent ATPase in human cells. Nucleic Acids Res. *31*, 6117–6126.

Shibata, A., Moiani, D., Arvai, A.S., Perry, J., Harding, S.M., Genois, M.M., Maity, R., van Rossum-Fikkert, S., Kertokalio, A., Romoli, F., et al. (2014). DNA double-strand break repair pathway choice is directed by distinct MRE11 nuclease activities. Mol. Cell *53*, 7–18. https://doi.org/10.1016/j.molcel.2013.11.003.

Sirbu, B.M., McDonald, W.H., Dungrawala, H., Badu-Nkansah, A., Kavanaugh, G.M., Chen, Y., Tabb, D.L., and Cortez, D. (2013). Identification of proteins at active, stalled, and collapsed replication forks using isolation of proteins on nascent DNA (iPOND) coupled with mass spectrometry. J. Biol. Chem. *288*, 31458–31467. https://doi.org/10.1074/jbc.M113.511337.

Taglialatela, A., Alvarez, S., Leuzzi, G., Sannino, V., Ranjha, L., Huang, J.W., Madubata, C., Anand, R., Levy, B., Rabadan, R., et al. (2017). Restoration of

replication fork stability in BRCA1− and BRCA2-deficient cells by inactivation of SNF2-family fork remodelers. Mol. Cell *68*, 414.e8. 430.e8. https://doi.org/10.1016/j.molcel.2017.09.036.

Taglialatela, A., Leuzzi, G., Sannino, V., Cuella-Martin, R., Huang, J.W., Wu-Baer, F., Baer, R., Costanzo, V., and Ciccia, A. (2021). REV1-Polζ maintains the viability of homologous recombination-deficient cancer cells through mutagenic repair of PRIMPOL-dependent ssDNA gaps. Mol. Cell *81*, 4008.e7. 4025.e7. https://doi.org/10.1016/j.molcel.2021.08.016.

Tirman, S., Quinet, A., Wood, M., Meroni, A., Cybulla, E., Jackson, J., Pegoraro, S., Simoneau, A., Zou, L., and Vindigni, A. (2021). Temporally distinct post-replicative repair mechanisms fill PRIMPOL-dependent ssDNA gaps in human cells. Mol. Cell *81*, 4026.e8. 4040.e8. https://doi.org/10.1016/j.molcel.2021.09.013.

Vaitsiankova, A., Burdova, K., Sobol, M., Gautam, A., Benada, O., Hanzlikova, H., and Caldecott, K.W. (2022). PARP inhibition impedes the maturation of nascent DNA strands during DNA replication. Nat. Struct. Mol. Biol. *29*, 329–338. https://doi.org/10.1038/s41594-022-00747-1.

Williams, R.S., Dodson, G.E., Limbo, O., Yamada, Y., Williams, J.S., Guenther, G., Classen, S., Glover, J.N., Iwasaki, H., Russell, P., and Tainer, J.A. (2009). Nbs1 flexibly tethers Ctp1 and Mre11-Rad50 to coordinate DNA double-strand break processing and repair. Cell *139*, 87–99. https://doi.org/10.1016/j.cell.2009.07.033.

Wist, E., and Prydz, H. (1979). The effect of aphidicolin on DNA synthesis in isolated HeLa cell nuclei. Nucleic Acids Res. *6*, 1583–1590. https://doi.org/10.1093/nar/6.4.1583.

Wood, R.D., and Doublié, S. (2016). DNA polymerase θ (POLQ), double-strand break repair, and cancer. DNA Repair *44*, 22–32. https://doi.org/10.1016/j.dnarep.2016.05.003.

Wyatt, D.W., Feng, W., Conlin, M.P., Yousefzadeh, M.J., Roberts, S.A., Mieczkowski, P., Wood, R.D., Gupta, G.P., and Ramsden, D.A. (2016). Essential roles for polymerase θ -mediated end joining in the repair of chromosome breaks. Mol. Cell *63*, 662–673. https://doi.org/10.1016/j.molcel.2016.06.020.

Yamaguchi-Iwai, Y., Sonoda, E., Sasaki, M.S., Morrison, C., Haraguchi, T., Hiraoka, Y., Yamashita, Y.M., Yagi, T., Takata, M., Price, C., et al. (1999). Mre11 is essential for the maintenance of chromosomal DNA in vertebrate cells. EMBO J. *18*, 6619–6629. https://doi.org/10.1093/emboj/18.23.6619.

Zarrizi, R., Higgs, M.R., Voßgröne, K., Rossing, M., Bertelsen, B., Bose, M., Kousholt, A.N., Rösner, H., Network, T.C., Ejlertsen, B., et al. (2020). Germline RBBP8 variants associated with early-onset breast cancer compromise replication fork stability. J. Clin. Invest. *130*, 4069–4080. https://doi.org/10.1172/JCI127521.

Zatreanu, D., Robinson, H.M.R., Alkhatib, O., Boursier, M., Finch, H., Geo, L., Grande, D., Grinkevich, V., Heald, R.A., Langdon, S., et al. (2021). Polθ inhibitors elicit BRCA-gene synthetic lethality and target PARP inhibitor resistance. Nat. Commun. *12*, 3636. https://doi.org/10.1038/s41467-021-23463-8.

Zhou, J., Gelot, C., Pantelidou, C., Li, A., Yücel, H., Davis, R.E., Färkkilä, A., Kochupurakkal, B., Syed, A., Shapiro, G.I., et al. (2021). A first-in-class polymerase theta inhibitor selectively targets homologous-recombination-deficient tumors. Nat. Cancer *2*, 598–610. https://doi.org/10.1038/s43018-021-00203-x.

STAR★METHODS

KEY RESOURCES TABLE

REAGENT or RESOURCE	SOURCE	IDENTIFIER
Antibodies		
Anti-ATR	Aze et al., 2016	N/A
Anti-BrdU (Mouse monoclonal)	BD Bioscience	Cat# ab347580, clone B44; RRID: AB_400326
Anti-BrdU (Rat monoclonal) [BU1/75 (ICR1)]	Abcam	Cat# ab6326; RRID: AB_305426
Anti-CDC45 (Rabbit polyclonal)	Aze et al., 2016	N/A
Anti-CtIP (Rabbit polyclonal)	Bethyl laboratories	Cat# A300-488A-M; RRID: AB_2779257
Anti-Histidine (Rabbit polyclonal)	Sigma-Aldrich	Cat# SAB4301134
Anti-Histone H2B (Rabbit polyclonal)	Millipore	clone 07-371; RRID: AB_310561
Anti-human POLα p180 (Rabbit polyclonal)	Abcam	Cat#ab31777; RRID:AB_731976
Anti-MCM7 (Mouse monoclonal)	Santa Cruz	Cat# sc-9966; RRID: AB_627235
Anti-MEK2 (Mouse monoclonal)	BD Bioscience	Cat# 610235; RRID: AB_397630
Anti-NBS1/NBN (Rabbit polyclonal)	Novus biologicals	Cat# NB100-143; RRID: AB_10078050
Anti-ORC1 (Mouse polyclonal)	Aze et al., 2016	N/A
Anti-phospho-Histone H2A.X-Ser139 (Mouse monoclonal)	Millipore	Cat# 05-636; RRID: AB_309864
Anti-PSF3 (Rabbit polyclonal)	Hashimoto et al., 2010	N/A
Anti-RAD51 (Mouse monoclonal) [14B4]	Abcam	Cat# ab213; RRID: AB_302856
Anti-RPA70 (Rabbit polyclonal)	Jean Gautier, Columbia University	N/A
Anti-*Xenopus* POL θ (Rabbit polyclonal)antigen used: His-POLθ $^{(1756-2542)}$	This study	BioGenes GmbH
Anti-*Xenopus* POL α p180 (Mouse monoclonal) peptide antigen used: VKRLPAVTKPGH	Kolinjivadi et al., 2017b	Abmart: clone 13026-1-3/C199
Anti-*Xenopus* POL δ 125 kDa (Mouse monoclonal) peptide antigen used: SSQTKKLRGDWDDD	Kolinjivadi et al., 2017b	Abmart: clone 19570-1-1/C316
Anti-*Xenopus* SMARCAL1 (Rabbit polyclonal) (*Xenopus* full length protein used as antigen)	Kolinjivadi et al., 2017b	N/A
Chicken anti-Rat IgG (H+L) Cross-Adsorbed Secondary Antibody, Alexa Fluor 488	ThermoFisher	Cat#A-21470; RRID:AB_2535873
Donkey Anti-Mouse IgG (H+L) Cy™3 AffiniPure	Jackson ImmunoResearch	Cat# 715-165-150; RRID: AB_2340813
Biological Samples		
Xenopus egg extract	This study	N/A
Chemicals, Peptides, and Recombinant Proteins		
3,5,8-Trimethylpsoralen TMP	Sigma-Aldrich	Cat# T6137
Aphidicolin	Sigma-Aldrich	Cat# A0781
Alkyldimethylbenzylammonium chloride	Merck	Cat# 264-151-6
Benzonase	Sigma-Aldrich	Cat# E1014
BrdU	Sigma-Aldrich	Cat# B5002
BSA	Sigma-Aldrich	Cat# A2058
Calcium ionophore	Sigma-Aldrich	Cat# A23187
CD437	Merck	Cat# C5865
CldU (5-chloro-2'-deoxyuridine)	Sigma-Aldrich	Cat# C6891
Corionic Gonadotropin	Sigma-Aldrich	Cat# CG10
DNA2i	MedChemExpress	Cat# HY-128729

(*Continued on next page*)

Continued

REAGENT or RESOURCE	SOURCE	IDENTIFIER
Dynabeads M-280 Streptavidin	ThermoFisher	Cat# 11205D
Dynabeads-ProteinA	ThermoFisher	Cat# 10002D
Formamide	Sigma-Aldrich	Cat# F9037
Geminin	Aze et al., 2016)	N/A
GST-BRC4 (residues $^{1511-1579}$ of human BRCA2)	Hashimoto et al., 2010)	N/A
Human Polymerase α^{1-1462} and B$^{1-598}$ subunit proteins	Kolinjivadi et al., 2017b	N/A
Human Primase His$_{10}$-tagged human Primase PriS and PriL subunit proteins	Kolinjivadi et al., 2017b	N/A
IdU (5-Iodo-2′-deoxyuridine)	Sigma-Aldrich	Cat# I7125
Lysolecithin	Sigma-Aldrich	Cat# L1381
Maltose	Sigma-Aldrich	Cat# M5885
MBP-tagged human Polymerase α^{1-109} NTD	Kolinjivadi et al., 2017b	N/A
Mirin	Sigma-Aldrich	Cat# M9948
Olaparib (AZD2281, Ku-0059436)	SelleckChem	Cat# S1060
PFM01	Sigma-Aldrich	Cat# SML1735
POLθ polymerase inhibitor (POLθi)	Joanna Loizou, University of Vienna	N/A
Protease inhibitor Set III	Calbiochem	Cat# 539134
Proteinase K	Sigma-Aldrich	Cat# 3115887001
PvuII HF restriction enzyme	NEB	Cat# R0151T
RNase A	ThermoFisher	Cat# EN0531
S1 nuclease	Sigma-Aldrich	Cat# N5661
Spermidine	Sigma-Aldrich	Cat# S2626
Spermine	Sigma-Aldrich	Cat# S3256
T4-DNA Polymerase	NEB	Cat# M0203S
TRIzol™ Reagent	Thermo Fisher	Cat# 15596026
Uranyl Acetate	Thermo Fisher	Cat# NC1375332
Xenopus Polθ-FL protein (His-MBP-TEV-Polθ$^{1-2542}$)	This study	N/A
Xenopus Polθ-HEL protein (His-MBP-TEV-POLθ$^{1-1029}$)	This study	N/A
Xenopus Polθ-POL protein (His-TEV-POLθ$^{1756-2542}$)	This study	N/A
Critical Commercial Assays		
15% TBE-Urea Polyacrylamide gel	Biorad	N/A
Amicon ultra centrifugal filters cut off 50kDa	Millipore	N/A
Midi-GeBaFlex (3.5 kDa MWCO)	GEBA	Cat# D012
ECL	Amersham	Cat# RPN2232
Gel Loading Buffer II	ThermoFisher	Cat# AM8546G
MBPTRAP™ HP	Cytiva	Cat# GE28-9187-79
Oligo(dT)20	Thermo Fisher	Cat# 18418020
pCR®-Blunt II-TOPO® vector	Invitrogen	Cat# K28002
Phusion™ High-Fidelity DNA Polymerase	Thermo Fisher	Cat# F530L
Superdex® 200 10/300 GL	Cytiva	Cat# 17-5175-01
Superose® 6 Increase 10/300 GL	Cytiva	Cat# GE29-0915-96
SuperScript™ III Reverse Transcriptase	ThermoFisher	Cat# 18080093
TALON® metal affinity resin	Clontech	N/A
Lipofectamine™ RNAiMax	ThermoFisher	Cat# 13778150
CellTiter-Glo® Luminescent Cell Viability Assay	Promega	Cat# G7571
Click-iT™ EdU Cell Proliferation Kit for Imaging, Alexa Fluor™ 488 dye	ThermoFisher	Cat# C10337

(Continued on next page)

Continued

REAGENT or RESOURCE	SOURCE	IDENTIFIER
Deposited Data		
Xenopus laevis Polθ cDNA	This study	GenBank: OM249942
Raw images and graphs	This study	https://doi.org/10.17632/5ynd7b8759.1
Experimental Models: Cell Lines		
High Five insect cells	Invitrogen	Cat# B85502
DLD-1 wild-type	Horizon	Cat# HD PAR-008
DLD-1 BRCA2 -/-	Horizon	Cat# HD 105-007
Experimental Models: Organisms/Strains		
Xenopus laevis females	Nasco	Cat# LM00535MX
Xenopus laevis males	Nasco	Cat# LM00715MX
Oligonucleotides		
POLQ-N2 GGGGAGACGATGCAGCAGATAAAG	This study	N/A
POLQ-C3 GCCTCCTACAAGTCAAAATCTTGCAG	This study	N/A
POLQ_for-aa1-XhoI CCGCTCGAGAATGCAGCA GATAAAGAAACAGCCCC	This study	N/A
POLQ_for-aa1756-XhoI CCGCTCGAGAGGCTT CACCTTGCAGCTCTCTCAG	This study	N/A
PolQ_rev-aa1029_NheI TAGGCTAGCCTAATTC CACTGGATTCCAATCATGGCC	This study	N/A
PolQ_rev-aa2542_NheI TAGGCTAGCCTACAA GTCAAAATCTTGCAGATCTCCCC	This study	N/A
Additional DNA oligos	See Table S1	N/A
NBS1/NBN siRNA oligo	Horizon	Cat# L-009641-00-0010
RBBP8 siRNA oligo	Horizon	Cat# L-011376-00-0010
MRE11A siRNA oligo	Horizon	Cat# L-009271-00-0010
Universal control siRNA oligo	Sigma-Aldrich	Cat# SIC001
Recombinant DNA		
ADA438-pCRBluntIITOPO-POLQ (FL)	This study	N/A
ADA444-pBAC-6H-MBP-POLQ (FL)	This study	N/A
ADA446-pF-6His-POLQ-polymerase (1756-2542)	This study	N/A
ADA447-pBAC-6H-MBP-POLQ-Helicase (1-1029)	This study	N/A
ADA448- pBAC-6H-MBP-POLQ-polymerase (1756-2542)	This study	N/A
pFBDM-His$_{10}$-tagged full length human Primase subunits PriL and PriS	Kolinjivadi et al., 2017b	N/A
Software and Algorithms		
Prism (version 9.3.0)	GraphPad	https://www.graphpad.com; RRID: SCR_002798
ImageJ (version 2.3.0/1.53f)	Freeware	https://imagej.net; RRID: SCR_003070
CellProfiler 4.1.3	Freeware	https://cellprofiler.org; RRID: SCR_007358
Jalview 2.11.2.3	Freeware	https://www.jalview.org/ RRID: SCR_006459
Clustal Omega 1.2.2.	Freeware	http://www.clustal.org/omega/ RRID: SCR_001591
Gatan Micrograph softwareSoftware	Gatan	N/A
Other		
Bioruptor	Diagenode	N/A
Electron microscopy grids	Ted Pella	Cat# 3HGC100
ChemiDoc MP	BioRad	N/A
EnVision microplate reader	PerkinElmer	N/A

Continued

REAGENT or RESOURCE	SOURCE	IDENTIFIER
Typhoon scanner	GE Healthcare	N/A
FEI Tecnai 20 EM microscope equipped with GATAN high-resolution camera	FEI+Gatan	N/A
MED20 evaporator	Leica	N/A
Leica TCS SP8-STED confocal microscope		
Olympus Upright BX61 fluorescence microscope		
Stratalinker equipped with 254 and 365 nm ultraviolet light bulbs	Stratagene	N/A
TLA100 rotor	Beckman	N/A

RESOURCE AVAILABILITY

Lead Contact
Further information and requests for resources and reagents should be directed and will be fulfilled by the lead contact, Prof Vincenzo Costanzo (vincenzo.costanzo@ifom.eu).

Materials Availability
Materials generated in this study will be made available upon request by the lead contact.

Data and code availability
- Original western blot and microscopy images are available on Mendeley Data as of the date of publication. The DOI is listed in the key resources table.
- The study does not report any original code.
- Any additional information related to the data reported in this paper will be made available upon request by the lead contact.

EXPERIMENTAL MODEL AND SUBJECT DETAILS

Xenopus laevis eggs
Eggs derived from *Xenopus laevis* frogs were used as an experimental model system. Collection of eggs from the female frogs was performed in a non-invasive way following chorionic gonadotropin (Sigma, CG10) injections. Once collected eggs were processed to obtain cytoplasm, which was incubated with sperm nuclei to start DNA replication reactions. Occasional surgical procedures were performed on the male frogs to harvest sperm nuclei. Experimental protocols were approved by the IFOM Animal Welfare committee and the Italian Ministry of Health. The number of animals used was kept to a minimum and was calculated taking into account the number eggs required to obtain the cytoplasmic extract needed for the experiments described. The animals were kept in highly regulated and monitored conditions with room and water temperature at 19 °C. Basic husbandry requirements were provided by the IFOM *Xenopus* facility.

Cell culture
Human DLD1 wild-type and DLD1 $BRCA2^{-/-}$ deficient cells used as model system were purchased at Horizon discovery. Cells were cultured in RPMI 1640 (Lonza) supplemented with 2 mM glutamine, 10% Fetal bovine serum (FBS) and penicillin-streptomycin (Pen-Strep). Cells were maintained at 37 °C and 5% CO2. Cells were transfected with siRNA oligos and experiments were performed 48 h after transfection. Efficacy of knockdown was checked with western blot performed 72 h after transfection. Cells were also treated with chemicals such as DMSO, POLθi or PFM01 for the times indicated in figure legend.

METHOD DETAILS

DNA constructs
The cDNA sequences encoding *Xenopus laevis* POLθ was obtained by RT-PCR, from RNA derived from *Xenopus* eggs with TRIzol™ Reagent (Thermo Fisher). SuperScript™ III Reverse Transcriptase (Thermo Fisher) and oligo(dT)20 was used for the first strand DNA synthesis. The full-length *polq* sequence was amplified by PCR using Phusion™ High-Fidelity DNA Polymerase (Thermo Fisher) and the primers PolQ-N2 and PolQ-C3 (see table). The PCR product was cloned into pCR®-Blunt II-TOPO® vector (Invitrogen) obtaining the pCRBluntIITOPO-POLQ(FL) ADA438 plasmid. The sequence was verified by sequencing using the primers listed in the table below, and was deposit in GenBank (BankIt2538668 POLQ OM249942). To obtain the pBAC-6H-MBP-POLQFL ADA444 plasmid,

for the expression in insect cells of the full-length sequence fused to 6His-MBP, a PCR product was obtained from ADA438 using the POLQ_for-aa1-XhoI and PolQ_rev-aa2542_NheI primers (see table). The PCR product was NheI/XhoI restricted and cloned into pBAC-His-MBP, a modified version of pFastBacHT vector, SalI/XbaI restricted. The sequence encoding the N-terminal helicase domain (aa1-1029) was amplified by PCR using the primers POLQ_for-aa1-XhoI and PolQ_rev-aa1029_NheI primers and cloned into the SalI/XbaI restricted pBAC-His-MBP vector, obtaining pBAC-6H-MBP-POLQ-Helicase$^{(1-1029)}$ (ADA447 plasmid). The sequence encoding the C-terminal polymerase domain (aa1756-2542) was amplified by PCR using the primers POLQ_for-aa1756-XhoI and PolQ_rev-aa2542_NheI and cloned into the SalI/XbaI restricted pFH1, a modified version of pFL vector, obtaining pF-6His-POLQ-polymerase$^{(1756-2542)}$ (ADA446 plasmid), or it was cloned into pBAC-His-MBP obtaining pBAC-6H-MBP-POLQ-polymerase$^{(1756-2542)}$ (ADA448 plasmid).

See Table S1 for complete list of DNA oligonucleotide primers used for cloning. All primers were purchased from SIGMA.

Protein expression and purification

His-MBP-TEV-POLθ$^{(1-2542)}$(FL), His-MBP-TEV-POLθ$^{(1-1029)}$ (helicase domain) and His-TEV- POLθ$^{(1756-2542)}$ (polymerase domain) were expressed in High Five insect cells (Invitrogen, B85502) infected with the respective recombinant baculoviruses by Silvia Monzani and Sebastiano Pasqualato of the Crystallography Unit of the European Institute of Oncology. Cell pellets from cells expressing His-MBP-TEV-POLθ$^{(1-2542)}$ (FL) and His-MBP-TEV-POLθ$^{(1-1029)}$ (Helicase domain) were resuspended in MBP-lysis buffer (50 mM HEPES pH 7.6, 300 mM NaCl, 1 mM DTT, 1 mM EDTA) supplemented with protease inhibitors cocktail Set III (Calbiochem) and 12.5 U/ml Benzonase (Sigma), lysed by sonication and cleared by centrifugation. The cleared lysate was loaded onto MBP-TRAP column (GE Healthcare), washed with 20 column volumes of washing buffer (50 mM HEPES pH 7.6, 300 mM NaCl, 1 mM EDTA, 5% glycerol); proteins were eluted with MBP-elution buffer (20 mM maltose, 50 mM HEPES pH 7.6, 200 mM NaCl, 1 mM EDTA, 5% glycerol). The eluate was further purified by SEC on Superose-6 column (GE Healthcare) pre-equilibrated in SEC buffer (50 mM HEPES, 200 mM NaCl, 5% glycerol). Relevant fractions were concentrated in 50 kDa molecular mass cut-off Amicon ultra centrifugal filters (Millipore).

Cell pellets from cells expressing 6xHis-TEV- POLθ$^{(1756-2542)}$ were resuspended in His-lysis buffer (50 mM HEPES pH 7.6, 300 mM NaCl, 10% glycerol, 2 mM 2-mercaptoethanol, 0.25% Triton X-100) supplemented with protease inhibitors cocktail Set III and 12.5U/ml Benzonase), lysed by sonication and cleared by centrifugation. The cleared lysate was incubated with TALON® metal affinity resin (Clontech) for 2h at 4 °C. The resin was then washed with 30 vol. of lysis buffer containing 500 mM NaCl and 10 mM Imidazole; the bound proteins were eluted with 300 mM imidazole in lysis buffer. The eluate was further purified by SEC on Superdex-200 column (GE Healthcare) pre-equilibrated in SEC buffer. Relevant fractions were concentrated in 50 kDa cut-off Amicon ultra centrifugal filters (Millipore).

Recombinant wild type human Polα complex used in this work was previously produced (Kolinjivadi et al., 2017b).

Antibody production

Anti-*Xenopus*-POLθ antibodies were obtained by BioGenes GmbH (Germany) by immunizing two rabbits (#29046 and #29047) with His-POLθ$^{(1756-2542)}$. The antibodies were affinity purified with His-MBP-POLθ$^{(1756-2542)}$ by Giuseppe Ossolengo (IFOM). The antibody #29046 was used for WB detection and #29047 for immunodepletion.

OLIGO extension assay and GAP-filling

To test the polymerase activity of POLθ we evaluated its capability to extend a tetra-chloro-fluorescein (TET) 5'-end labelled oligo (14mer) annealed to a reverse oligonucleotide (21mer or 41mer) see table. To obtain the ds-duplex 5' protruding template, we mixed 1 μM of TET-14mer-forward oligonucleotide and 2 μM of either 21mer_reverse or 41mer_reverse oligonucleotide in annealing buffer (10 mM Tris–HCl pH 8, 50 mM NaCl, 0.1 mM EDTA) and annealed by heating at 95 °C for 5 min and slowly cooling down to 25 °C. For the polymerase reaction we prepared a 10 μl mix containing 50 nM ds-template, 100 μM dNTPs and 50 nM POLθ (either 6H-MBP-POLθ-FL or 6H-POLθ-POL) in reaction buffer (20 mM Tris-HCl buffer, pH 8.0, 25 mM KCl, 10 mM MgCl$_2$, 1 mM DTT). The reaction was incubated at 37 °C for 15-30 min and quenched by adding 100 mM NaOH and 10 μl of Gel Loading Buffer II (Thermo Fisher, AM8546G) containing 95% formamide, 18 mM EDTA, and heating for 5 min at 95 °C. Products were separated on denaturing 15% Polyacrylamide-8M Urea gels in 1xTBE buffer and visualized on ChemidocMP (Bio-Rad) using blue epi-illumination and the 530/28 emission filter. As standard-ladder we used a mix of TET14mer, TET-20mer, TET-24mer, TET-30mer andTET-40mer oligonucleotides, 5 nM each in Gel Loading Buffer II.

For the GAP-filling assay we prepared the two templates: NO-GAP and GAP-8 templates. The NO-GAP template was obtained by annealing the TET-15mer_forward with the 51mer_reverse (at the ratio of 1:1.5). The GAP-8 template was obtained by the annealing of the TET-15mer_forward with the 51mer_reverse and the GAP8-18mer-CY3_forward (at the ratio of 1:1.5:2). The templates were purified from a native 6% PAGE gel and extracted by electroelution using the midi GeBaFlex (3.5 kDa MWCO) tubes. For the reaction we prepared a 10 μl mix containing 50 nM template, 100 μM dNTPs in reaction buffer supplemented with 1 mM ATP to which we added either 50 nM 6H-MBP-POLθ-FL or 0.1 U of T4-DNA Polymerase (NEB). The reaction was incubated at 23 °C for 30 min.

For the complete sequence of DNA oligos used here see Table S1.

Egg extract and chromatin binding

Xenopus interphase egg extracts and sperm nuclei were prepared as previously described (Aze et al., 2016). Briefly, *Xenopus* eggs were collected in MMR buffer (5 mM HEPES-KOH pH 7.5, 100 mM NaCl, 0.5 mM KCl, 0.25 mM MgSO$_4$, 0.5 mM CaCl$_2$, 25 μM EDTA) from chorionic gonadotropin injected female frogs. The eggs were de-jellied in 10 mM Tris pH 8.0, 110 mM NaCl and 5 mM DTT and rinsed three times in MMR. De-jellied eggs were released in interphase in presence of 5 μM Calcium Ionophore (A23187, Sigma) for 5-6 min, washed three times with MMR and rinsed twice in ice-cold S-buffer (50 mM HEPES-KOH pH 7.5, 50 mM KCl, 2.5 mM MgCl$_2$, 250 mM sucrose, 2 mM β-mercaptoethanol). Activated eggs were then packed by centrifugation at 1.200 rpm for 1 min and the excess of buffer was discarded. Eggs were crushed at 13.000 rpm for 12 min at 4 °C. The crude extract was collected and centrifuged at 70.000 rpm for 12 min at 4 °C in a TLA100 rotor (Beckman). The interphase extract was obtained by collecting and mixing the cleared cytoplasmic fraction together with the nuclear membranes. For sperm nuclei preparation 4 testis were removed from 2 male frogs and placed in petri dishes containing 10 mL EB buffer (50 mM KCl, 50 mM HEPES-KOH pH 7.6, 5 mM MgCl$_2$, 2 mM DTT). Testis were finely chopped with razor blade. The material was then transferred to 15 mL Falcon tube and spun at 2,000 x g, in a swinging bucket rotor for 5 min at 4 °C. The pellet was resuspended in a total volume of 2 mL of room temperature SuNaSp buffer (0.25 M sucrose, 75 mM NaCl, 0.5 mM spermidine, 0.15 mM spermine). To remove membranes 100 μl of 2 mg/ml lysolecithin (Sigma) were added and incubated for 10 min at room temperature. Reaction was stopped by adding 3% BSA (Sigma). The pellet was re-suspended again in 2 mL EB and spun at 2,000 x g for 5 min at 4 °C. The final pellet was resuspended in 400 μl of EB + 30% glycerol. Sperm nuclei were tested for absence of DNA breaks with TUNEL assay as previously described (Aze et al., 2016). Briefly, 20 μl of different sperm nuclei preparations (4000 n/μl) were incubated at 37 °C for 4 h in 170 μl H$_2$O supplemented with 20 μl 10 x TdT buffer (NEB), 90U Terminal transferase (NEB) and 1 μl α-^{32}P-dCTP. Aliquots of the reaction were then precipitated with 5% TCA, 2% py-rophosphate solution and spotted on Whatman GF-C glass fiber filter. After ethanol washes, filters were dried and the incorporated TCA precipitable radioactivity was counted in scintillation counter. Sperm nuclei preparations with the lowest counts were used for all the experiments.

The DNA replication assay was performed as previously described (Aze et al., 2016). Briefly, sperm nuclei (4000 n/μl) were added to interphase egg extract treated as shown in Figure legend. Extracts were supplemented with α-^{32}P-dCTP, incubated at 23 °C for the times indicated in figure legend and then stopped with Stop buffer (1% SDS, 8 mM EDTA, 80 mM Tris-HCl pH 8 and 1 mg/ml proteinase K). The mixture was then incubated at 50 °C for 2 h. Genomic DNA was separated from unincorporated nucleotides by electrophoresis through a 0.8% agarose gel. The gel was fixed in 30% TCA for 20 min, dried and exposed for autoradiography to a phosphoscreen for imaging acquisition using a phospho-imager scanner (Typhoon, GE Healthcare). Images were quantified with ImageJ software.

For chromatin binding 40 μl egg extract containing sperm DNA were isolated from master reactions treated as shown in Figure legends at the indicated time points. For immunoblotting, samples were diluted with 10 volumes of EB (100 mM KCl, 2.5 mM MgCl$_2$, and 50 mM HEPES–KOH pH 7.5) containing 0.25% NP-40 and centrifuged through a 0.5 M sucrose layer at 10,000 x g at 4 °C for 5 min. Pellets were washed once with EB and suspended in Laemmli loading buffer. Proteins were then resolved on an SDS-PAGE and monitored by WB.

DNA Electron microscopy

DNA for electron microscopy analysis was processed as previously described with some modifications (Kolinjivadi et al., 2017b; Taglialatela et al., 2017, 2021). Briefly, for *Xenopus* replication intermediates preparation sperm nuclei (4000 n/μl) were incubated at 23 °C in 200 μl egg extract for 60 min, diluted with 400 μl of EB buffer, layered onto 800 μl EB-EDTA (EB buffer + 1 mM EDTA) + 30% (w/v) sucrose and centrifuged at 3,000 x g for 10 min at 4 °C. Pellets were resuspended in 100 μl EB-EDTA and transferred to a 96-well plate. 4,5′,8-Trimethylpsoralen (TMP) was added at 10 μg/ml to each well. For human cells replication intermediates preparation 15x10^6 cells were collected. After standard trypsinization, the cells were transferred to 15 ml Falcon tubes and spun down at 600 x g for 5 min at 4°C. The cell pellets were then washed once with 5 ml ice-cold PBS, resuspended in 10 ml ice-cold PBS and transferred to 10x5 mm Petri dishes, to which 10 mg/ml of TMP (Trimethylpsoralen, Sigma-Aldrich) were added and mixed. *Xenopus* or human samples were incubated on ice for 5 min in the dark and irradiated with 365 nm ultraviolet light for 7 min on a precooled metal block. The procedure from TMP addition to irradiation with ultraviolet light was repeated four more times. Samples were then supplemented with 0.1% (w/v) SDS to lysate nuclei and treated with 100 μg/ml RNase A for 1 h at 37 °C. For complete protein diges-tion, psoralen-crosslinked chromatin was incubated with proteinase K (1 mg/ml) for 2 h at 50 °C. Genomic DNA was extracted by adding one volume of 1:1 (v/v) phenol–chloroform mixture, precipitated with isopropanol, washed with 70% ethanol and digested with 150 U PvuII HF restriction enzyme for 4 hours at 37 °C. To visualize DNA the samples were spread onto EM grids and stained as previously described (Kolinjivadi et al., 2017b; Taglialatela et al., 2017). Briefly, 50 ng DNA were resuspended in 5 μl of formamide supplemented with 0.4 μl of BAC solution (alkyldimethylbenzylammonium chloride 0.2% w/v in formamide) diluted 1:10 (v/v) in water. The total volume was gently pipetted onto the surface of water in a Petri dish to form a film. DNA was transferred to carbon-coated EM grids (Ted Pella) by briefly allowing them to contact the surface of the DNA film using tweezers. After staining in 1% uranyl acetate solution followed by a brief wash in 100% ethanol, grids were air-dried on filter paper and then subjected to DNA carbon-platinum rotary shadowing with a Leica MED20. Image acquisition was obtained with a FEI Tecnai 20 EM microscope equipped with a GATAN high-resolution camera at the IFOM electron microscopy facility. Blind analysis of EM images was performed by EM specialists. Conversion of DNA length from nm to nucleotides was done considering 1 nt=0.34 nm under EM.

Depletions

To immuno-deplete POLθ and SMARCAL1 0.5-1 mL egg extract were incubated with affinity purified IgGs (35-50 μg) at RT for 1 h with 250 μl Dynabeads-ProteinA (Thermo Fisher, 10002D) for one to three subsequent depletion rounds lasting about 1 h each.

To obtain mock-treated extract a parallel depletion was carried out using the same protocol with Dynabeads-ProteinA conjugated with affinity purified rabbit pre-immune IgGs.

IPOND

100 μl extracts were used for each sample. Sperm nuclei were then added to reach a final concentration of 4000 nuclei/μl. 30 min after sperm nuclei addition 10 min DNA labeling pulses were carried out supplementing the extracts with 40 μM Biotin-16-dUTP (Roche) and either 20 μM aphidicolin or DMSO as control. DNA replication was stopped by diluting 100 μl reactions with 200 μl cold EB-EDTA buffer (50 mM HEPES-KOH pH 7.5, 100 mM KCl, 2.5 mM MgCl$_2$, 1 mM EDTA). Samples were homogenized by using a cut p1000 tip and overlaid on 600 μl EB-EDTA-Sucrose buffer (EB-EDTA buffer + 30% w/v sucrose). Nuclei were collected by centrifugation at 8,300 x g at 4 °C for 10 min in a swinging-bucket rotor (TLA 100.3, Beckman). The supernatant and the dense sucrose layer were carefully removed and the nuclear pellet resuspended with 400 μl EB-NP40 buffer (50 mM HEPES-KOH pH 7.5, 100 mM KCl, 2.5 mM MgCl$_2$, 0.25% NP40) to lysate nuclei. Samples were then subjected twice to a 10 min sonication step (30 s ON / 40 s OFF cycle and Max Power with a Bioruptor device, Diagenode). After the sonication step 20 μl from each sample were kept apart (5% Input to be loaded as control for SDS-PAGE). Biotinylated DNA fragments were then pulled-down by incubation with 40 μl Dynabeads M-280 Streptavidin (Thermo Fisher, 11205D) for 30 min at 4 °C. Dynabeads M-280 Streptavidin + the pull-down fractions were then washed three times with 200 μl EB-EDTA buffer and eventually resuspended with 30 μl of 1X denaturing loading buffer. The entire volume was eventually loaded on for SDS-PAGE and WB analysis.

RNA Interference

siRNA transfections were performed using Lipofectamine™ RNAiMax (ThermoFisher, 13778150) following manufacturer's instructions. The final concentration of siRNA was 25 nmol/L. The siRNAs used were siNBN (L-009641-00-0010), siRBBP8 (CtIP, L-011376-00-0010) and siMRE11A (L-009271-00-0010) from Horizon, and universal control siRNA (SIC001) form Sigma. siRNA efficiency was assayed by western blot 72 h after transfection.

Immunofluorescence

Immunofluorescence was performed on siRNA transfected or un-transfected cells seeded on a glass coverslip. For drug treatment 24 later cells were exposed to DMSO or 2 μM POLQ inhibitor plus or minus 10 μM PFM01 for 24 h as indicated in figure legend. Cells then were exposed to 10 mM of EdU for 90 min then cells were washed once with PBS and pre-extracted with CSK100 buffer (100 mM NaCl, 10 mM PIPES pH 6.8, 3mM MgCl$_2$, 300 mM sucrose, 0.5% Triton X-100) for 2 min on ice. Cells were washed once with PBS and Fixed with 4% formaldehyde in PBS for 12 min at room temperature. Permeabilized with permeabilization buffer (0.2% BSA, 0.5% Triton X-100 in PBS) for 10 min, washed once with PBS and EdU-positive cells were detected with Click-it EdU Cell Proliferation Kit (Thermo Fisher) following manufacturer's instructions. Cells were blocked with blocking solution (10 mM Glycine, 2 %BSA, 0.2 % gelatin, 50 mM NH$_4$Cl, 0.2%Triton X-100) for 1 h at room temperature. Coverslips were incubated with primary antibody for 1h at 37 °C, washed 3 times with PBS and then incubated the secondary antibody. After 3 washed with PBS coverslips were incubated with 5 μg/mL DAPI in PBS for 10 min, washed once and mounted in Vectashield plus (Vector labs) and stored at 4°C until image acquisition.

Confocal fluorescent cell images were acquired with a Leica TCS SP8-STED confocal microscope with HC PL APO CS2 63x/1,40 oil (Figures 6D and S7H) or HC PL APO 40x/1,30 oil (Figures S7E and S7K) objective a 60X oil immersion objective 1.35 NA or 40X oil immersion objective. Wide field fluorescent cell images were acquired with an Olympus Upright BX61 fluorescence microscope with a 60X oil immersion objective 1.35 NA. At least 10 images were capture per condition and more than 500 nuclei were analyzed with CellProfiler 4.1.3.

DNA fiber analysis

Asynchronously growing cells were seeded in 6-well dishes; 24h later cells were pulse labeled with 25 μM CldU (Sigma) for 20 min, washed twice with warm PBS and then labeled with 250 μM IdU (Sigma) for 40 min. POLθi was present for the time indicated in figures legend during the whole labeling time. Cells were trypsinized, counted and resuspended at a final concentration of 1-2x10^3 cell/μL. The cell suspension (2 μl) was lysed on a clean glass slide with 8 μl MES lysis buffer (500 mM MES pH 5.6, 0.5% SDS, 50 mM EDTA, 100 mM NaCl) for 7 min. The slide was then tiled at a 15° angle to allow the DNA to spread. Slides were air-dried for 30 min, fixed in freshly prepared acetic acid/methanol (1:3) for 10 min, air-dried again and stored at 4 °C overnight.

Slides were rehydrated with PBS 1X for 5 min, DNA was denatured with 2.5 M HCl for 80 min, slides were washed several times with PBS, and finally blocked in blocking solution (5% BSA, 0.2% Triton X-100 in PBS) for 20 min. For fiber visualization slides were incubated with primary antibody mix in blocking solution using anti-BrdU (6326, Abcam), which recognizes CldU at 1:100 dilution, and anti-BrdU (347580, BD biosciences), which recognizes IdU at 1:50 dilution. The reactions were incubated for 90 min at 37 °C in a humid chamber. After incubation, slides were washed once with 0.1% Tween in PBS and twice with PBS for 3 min each. Slides were then incubated with secondary antibody mix using fluorescent donkey anti-mouse CY3 (715-165-150, Jackson ImmunoResearch) and chicken anti-rat immunoglobulins (A-21470, Thermo Fisher) in blocking solution for 45 min at 37 °C degrees

in a humid chamber. Slides were washed 3 times in PBS, air-dried, mounted in Vectashield plus (Vector labs) and stored at 4 °C until image acquisition. Images were acquired with an Olympus Upright BX61 fluorescence microscope with a 60X oil immersion objective 1.35 NA. Depending on fiber density 5 to 10 images were capture for each treatment condition and at least 200 fibers were measured using ImageJ software version 2.3.0/1.53f.

S1 assay

The S1 assay was conducted as previously described (Taglialatela et al., 2021). Briefly, asynchronous cells were seeded in 6-well dishes, 24 h later cells were pulse labeled with 25 μM CldU (Sigma) for 20 min, washed twice with warm PBS and then labeled with 250 μM IdU (Sigma) for 40 min. When indicated, the cells were treated during the second pulse with POLθi (2 μM), Mirin (50 μM) or PFM01 (50 μM).Cells were washed once with PBS and then permeabilized with CSK100 buffer (100 mM NaCl, 10 mM PIPES pH 6.8, 3mM MgCl$_2$, 300 mM sucrose, Triton 0.5% X-100) for 8 min at room temperature. Exposed nuclei were washed once with S1 buffer (30 mM Sodium acetate pH 4, 2 mM Zinc sulphate, 50 mM NaCl, 5% glycerol) and then incubated with 10 U/mL of S1 nuclease (Sigma) in S1 buffer for 15 min at 37 °C. Nuclei were scrapped in 1 mL of PBS 0.1% BSA, centrifugated 5 min at 7.000 rpm and resuspend in PBS to a final concentration of 1-2x10^3 nuclei/μL. DNA was spread and stained as described above.

Cell viability assay

For viability assays cells were seeded in a 96 well plates at density of 2x10^3 cells/well. POLθi was added 24 h later after siRNA transfection when indicated at the concentrations indicated in the figure. Five days after, viability was determined CellTiter-Glo Luminescent Cell Viability Assay (Promega) following manufacturer instructions. Luminescence was measured in a microplate reader (EnVision, Perkin Elmer) and normalized as above. Relative cell viability (%) was expressed as a percentage relative to the untreated (DMSO) cells. Each viability experiment was performed three times.

Reagents

Aphidicolin was used at a concentration of 1.5 mM (APH) or 20 μM (M-APH) as indicated in figure legends. Geminin (60 nM) was used as previously described (Hashimoto et al., 2010). POLθ proteins were used at 25 nM. Mirin (M9948) and PMF01 (SML1735) were from SIGMA. DNA2i (HY-128729) was obtained from MedChemExpress. Cell lines DLD1 wild-type (HD PAR-008) and DLD1 *BRCA2$^{-/-}$* (HD 105-007) were from Horizon.

POLθi was obtained from the lab of J. Loizou and was synthesized according to the structure derived from two patents (Blencowe et al., 2020a, 2020b).

POLθi, DNA2i, Mirin and PFM01 were used at the concentrations indicated in the text and figure legend.

Antibodies

Anti-*Xenopus* proteins antibodies, except anti-POLθ, were previously described (Aze et al., 2016) (Kolinjivadi et al., 2017b). Rat monoclonal [BU1/75 (ICR1)] antibodies to BrdU (ab6326) were purchased from Abcam. Purified Mouse Antibodies against BrdU (B44) (347580) were from BD bioscience. Mouse Anti-phospho-Histone H2A.X-Ser139 antibody was from Millipore (05-636). Anti-histidine was obtained from Sigma (SAB4301134).

Software Availability

The following software was used:

GraphPad Prism (version 9.3.0)	https://www.graphpad.com;
ImageJ version 2.3.0/1.53f	https://imagej.net
CellProfiler 4.1.3.	https://cellprofiler.org
Jalview 2.11.2.3.	https://www.jalview.org/
Clustal Omega 1.2.2.	http://www.clustal.org/omega/

QUANTIFICATION AND STATISTICAL ANALYSIS

Statistical analysis

All experiments, if not indicated otherwise in the figure legend, were performed three times and representative experiments are depicted. No statistical methods or criteria were used to estimate sample size or to include/exclude samples. Statistical analysis was performed with GraphPad PRISM software (version 9.3.0). Statistical differences in the DNA fiber analyses and S1 nuclease assay were determined using Kruskal-Wallis test. Unpaired t-tests were used to assess the difference in means of two groups of data. In all cases, ns indicates not significant, *P<0.05, **P<0.01, ***P<0.001 and ****P<0.0001. Image analysis was conducted using ImageJ and CellProfiler 4.1.3. Statistical details for each experiment including sample size, significance values and tests are indicated in figure legends and figures.